Electronic Supplementary Material (ESI) for ChemComm.

Photo-Induced Formation of Organic Nanoparticles with Possessing Enhanced Affinites for Complexing Nerve Agent Mimics

Sarah E. Border,[a] Radoslav Z. Pavlović,[a] Lei Zhiquan,[a] Michael J. Gunther,[a] Han Wang,[b] Honggang Cui[b] and Jovica D. Badjić [a]*

[a]Department of Chemistry and Biochemistry, The Ohio State University, 100 West 18th Avenue, Columbus, OH 43210; [b]Department of Chemical and Biomolecular Engineering, The Johns Hopkins University, Maryland Hall 221, 3400 North Charles Street, 21218 Baltimore, Maryland USA.

E-mail: badjic.1@osu.edu

SUPPORTING INFORMATION

CONTENTS

General Information

All chemicals were purchased from commercial sources and used as received unless stated otherwise. All solvents were dried prior to use according to standard literature procedures. Chromatographic purifications were performed with silica gel 60 (SiO_2, Sorbent Technologies 40-75μm, 200 x 400 mesh). Thin-layer chromatography (TLC) was performed on silica-gel plate w/UV254 (200 μm). Chromatograms were visualized by UV-light or stained with I_2 in SiO_2. All NMR samples were contained in class B glass NMR tubes (Wilmad Lab Glass). NMR experiments were performed with Bruker 600, 700 and 850 MHz spectrometers. Chemical shifts are expressed in parts per million (δ, ppm) while coupling constant values (J) are given in Hertz (Hz). Residual solvent protons were used as internal standards: for ^{1}H NMR spectra $CDCl_3$ = 7.26 ppm, $(CD_3)_2SO$ = 2.50 ppm and D_2O = 4.79 ppm while for ^{13}C NMR spectra $CDCl_3$ = 77.0 ppm and $(CD_3)_2SO$ = 41.23 ppm; $CDCl_3$, D_2O, and $(CD_3)_2SO$ were purchased from Cambridge Isotope Laboratories. HRMS data was measured on a Bruker-ESI TOF instrument. All UV-Vis spectra were recorded on Shimadzu UV-2401 PC UV-Vis Spectrophotometer in 30 mM phosphate buffer at pH = 7.0 ± 0.1. All DLS measurements were completed (in triplicate) on a Malvern Zetasizer Nano Z6 instrument in 30 mM phosphate buffer at pH = 7.0 ± 0.1 which was filtered three times (0.22μm) prior to immediate use. The measurements of pH were completed with an HI 2210 pH meter. All photochemical experiments were completed by placing NMR tubes (containing a reaction mixture) in a Rayonet chamber reactor (RPR-100) equipped with sixteen RPR-3000A bulbs (300 nm). Specimens for cryo-TEM imaging were prepared using Vitrobot (FEI, Hillsboro, OR). All TEM grids used for cryo-TEM imaging were pretreated with plasma air to render the lacey carbon film hydrophilic. Samples $\mathbf{4}^{3-}$, $\mathbf{5}^{3-}$, and $\mathbf{6}^{3-}$ were imaged at a concentration of ca. 1.0 mM in 30 mM phosphate buffer at pH = 7.0 ± 0.1. 5 μL of the sample solution (with or without ten molar equivalents of DMPP) was loaded onto a copper grid coated with lacey carbon film (Electron Microscopy Sciences, Hatfield, PA) in a controlled humidity chamber and subsequently blotted by two pieces of filter paper from both sides of the grid. This process engenders a thin film of solutions (typically ~300nm). The blotted samples were then plunged into liquid ethane that was precooled by liquid nitrogen. The vitrified samples were stored in liquid nitrogen before cryo-TEM imaging. To prevent sublimation, crystallization, and melting of the vitreous ice film, the cryo-holder temperature was maintained below -170°C during the entire imaging process. Cryo-TEM imaging was conducted on a FEI Tecnai 12 TWIN electron microscope operating at a voltage of 100 kV. Cryo-TEM micrographs were acquired using a 16-bit 2K×2K FEI Eagle bottom mount camera.

Synthetic Procedures

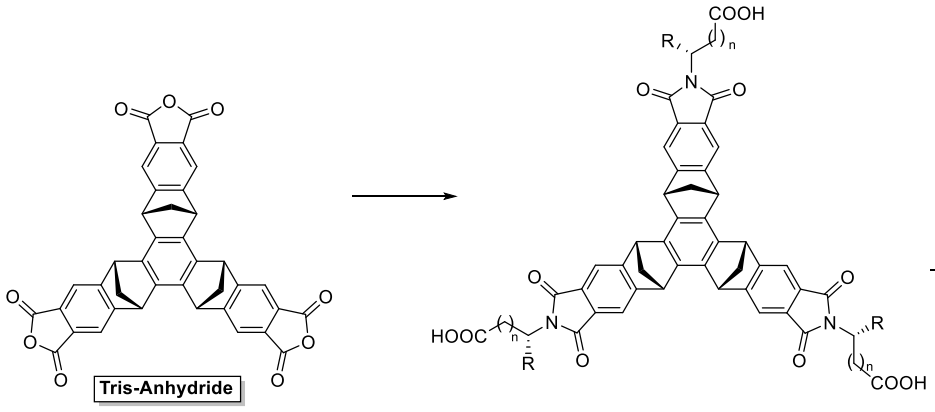

Basket	n	R (yield)
1*	1	COOH (92%)
3	3	COOH (76%)
4	1	H (93%)
6	3	H (82%)

Basket 1: Tris-Anhydride[1] (10 mg, 0.016 mmol) was dissolved in 1.2 mL of DMSO (Acros, 99.7 extra dry). To this solution, (*S*)-aspartic acid (21 mg, 0.16 mmol) and 1 µL glacial acetic acid were added and the mixture was heated to 120°C overnight under an atmosphere of nitrogen. Following, the solution was concentrated under reduced pressure, dissolved in water and the product was precipitated with 1M HCl. The precipitate was rinsed with distilled water (3 x 2 mL) to give basket **1** as a white solid (14.4 mg, 92%). ^{1}H NMR (850 MHz, CD_3SOCD_3): δ (ppm) 7.81-7.79 (m, 6H, H_C-type protons), 4.97-4.95 (m, 3H, H_A-type protons), 4.75 (s, 6H, $H_{D/D'}$-type protons), 3.02-2.99 (m, 3H, H_B-type protons), 2.67-2.61 (m, 3H, $H_{B'}$-type protons), 2.51 (m, 6H, $H_{E/F}$-type protons; ^{13}C NMR (212.5 MHz, CD_3SOCD_3): δ (ppm) 34.0 (C-3), 47.6 (C-2), 48.4 (C-9), 65.5-65.0 (C-11), 116.4-116.3 (C-7), 129.5 (C-6), 137.9 (C-12), 157.2 (C-8), 167.0-167.2 (C-5), 169.9-169.8 (C-4), 171.4 (C-1).HRMS (ESI-MS): *m*/z calcd for $C_{51}H_{33}N_3NaO_{18}$: 998.8178 $[M+Na]^+$; found: 998.1651. For the assignment of protons, see Figure 2A in the main text, while for carbons see Figure below; see also Figures S1-S3.

During the condensation, racemization at the α-position of aspartic acid occurred so that basket **1** was obtained as a mixture of, allegedly, two diastereomers **(*S*)$_3$-1** and **(*S,S,R*)-1**. Note that **(*S*)$_3$-1** is a C_3 symmetric molecule having three stereochemically identical arms. With one stereocenter within each arm, the corresponding H and C nuclei become chemically non-equivalent with different ^{1}H and ^{13}C NMR chemical shifts. On the other hand, diastereomer **(*S,S,R*)-1** possesses C_1 symmetry with fully desymmetrized scaffold. That is to say,

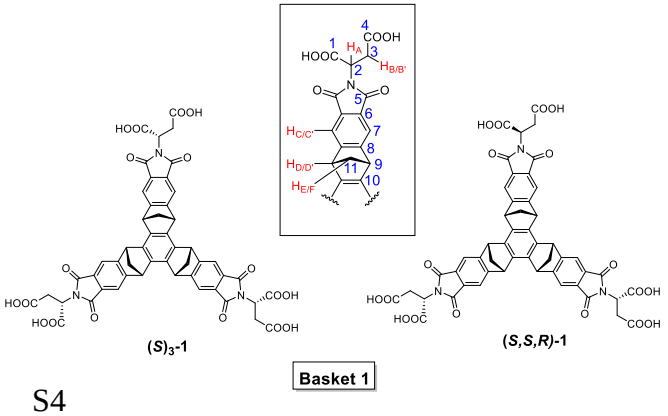

every proton and carbon nuclei are in this diastereomer expected to have a unique chemical shift. As the NMR signals from $^{1}H/^{13}C$ nuclei were clustered, we hereby report a range of chemical shifts.

Basket 3: Tris-Anhydride[1] (5.0 mg, 0.008 mmol) was dissolved in 0.6 mL of DMSO (Acros, 99.7 extra dry). To the solution, (*S*)-2-aminoadipidic acid (13 mg, 0.079 mmol) and 1 µL glacial acetic acid were added and the mixture was heated to 120°C overnight under an atmosphere of nitrogen. Following, the solution was concentrated under reduced pressure, dissolved in water and the product was precipitated with 1M HCl. The precipitate was rinsed with distilled water (3 x 2 mL) to give basket **3** as a white solid (6.4 mg, 76%). ^{1}H NMR (600 MHz, CD_3SOCD_3): δ (ppm) 12.43 (br. s, 6H, COO**H**), 7.821 (s, 3H, H_E), 7.818 (s, 3H, $H_{E'}$), 4.74 (s, 6H, $H_{F/F'}$), 4.55 (dd, J = 10.5 and 4.8 Hz, 3H, H_A), 2.50 (m, 6H, $H_{G/H}$), 2.11 (m, J = 7.0 Hz, 6H, $H_{D/D'}$), 2.02 (m, 3H, H_B), 1.91 (m, 3H, $H_{B'}$), 1.36 (m, 6H, $H_{C/C'}$); ^{13}C NMR (150 MHz, CD_3SOCD_3): δ (ppm) 21.2 (C-4), 27.5 (C-3), 32.7 (C-5), 48.3 (C-11/11'), 51.0 (C-2), 65.6 (C-13), 116.3 (C-9/9'),129.37 and 129.41 (C-8/8'), 137.7 (C-12/12'), 157.9 (C-10/10'), 167.32 and 167.42 (C-7/7'), 170.4 (C-1), 174.1 (C-6). HRMS (ESI-MS): *m*/z calcd for $C_{57}H_{45}N_3NaO_{18}$: 1082.2596 $[M+Na]^+$; found: 1082.2590; for $^{1}H/^{13}C$ NMR assignment of proton and carbon nuclei, see Figures S4-S7.

Basket 4: Tris-Anhydride[1] (7.0 mg, 0.011 mmol) was dissolved in 2 mL of glacial acetic acid. β-Alanine (3.3 mg, 0.037 mmol) and Cs_2CO_3 (10.8 mg, 0.033 mmol) were added and the mixture was heated to 120°C overnight under an atmosphere of nitrogen. Following, the solution was concentrated under reduced pressure, dissolved in water and the product was precipitated with 1M HCl. The precipitate was rinsed with distilled water (3 x 2 mL) to give basket **4** as a white solid (8.71 mg, 93%). ^{1}H NMR (700 MHz, CD_3SOCD_3): δ (ppm) 12.21 (br. s, 3H, COO**H**), 7.76 (s, 6H, H_C), 4.70 (s, 6H, H_D), 3.61 (t, J = 7.4 Hz, 6H, H_A), 2.50 (m, 6H, $H_{E/F}$ - overlapped with solvent residual signal; assigned from HSQC) 2.44 (t, J = 7.4 Hz, 6H, H_B); ^{13}C NMR (175 MHz, CD_3SOCD_3): δ (ppm) 32.4 (C-2), 33.3 (C-3), 48.2 (C-8), 65.2 (C-9), 116.0 (C-6), 129.8 (C-5), 137.9 (C-10), 157.6 (C-7), 167.6 (C-4), 172.0 (C-1). HRMS (ESI-MS): *m*/z calcd for $C_{48}H_{33}N_3NaO_{12}$: 866.1962 $[M+Na]^+$; found: 866.1956; for $^{1}H/^{13}C$ NMR assignment of proton and carbon nuclei, see Figures S8-S10.

Basket 6: Tris-Anhydride[1] (10.0 mg, 0.0158 mmol) was dissolved in 2 mL of glacial acetic acid. To this solution, 5-aminopentanoic acid (28 mg, 0.239 mmol) and Cs_2CO_3 (10.8 mg, 0.033 mmol) were added and the mixture was heated to 120°C overnight under an atmosphere of nitrogen. Following, the solution was concentrated under reduced pressure, dissolved in water and the product was precipitated with 1M HCl. The precipitate was rinsed with distilled water (3 x 2 mL) to give basket **6** as a white solid (12 mg, 82%). ^{1}H NMR (700 MHz, CD_3SOCD_3): δ (ppm) 11.96 (br. s, 3H, COO**H**), 7.75 (s, 6H, H_E), 4.70 (s, 6H, H_F), 3.37 (t, J = 6.7 Hz, 6H, H_A), 2.50 (m, 6H, $H_{G/H}$ - overlapped with solvent residual signal; assigned from HSQC), 2.16 (t, J = 7.0 Hz, 6H, H_D), 1.45 (quint, J = 7.5 Hz 6H, H_B), 1.39 (quint, J = 7.5 Hz 6H, H_C); ^{13}C NMR (175 MHz, CD_3SOCD_3): δ (ppm) 21.8 (C-3), 27.4 (C-4), 33.0 (C-2), 36.9 (C-5), 48.2 (C-10), 65.1 (C-12), 116.0 (C-8), 129.7 (C-7), 137.9 (C-11), 157.5 (C-9), 167.9 (C-6), 174.2 (C-1). HRMS (ESI-MS): *m*/z calcd for $C_{54}H_{45}N_3NaO_{12}$: 950.2901 $[M+Na]^+$; found: 950.2895; for $^{1}H/^{13}C$ NMR assignment of proton and carbon nuclei, see Figures S11-S14.

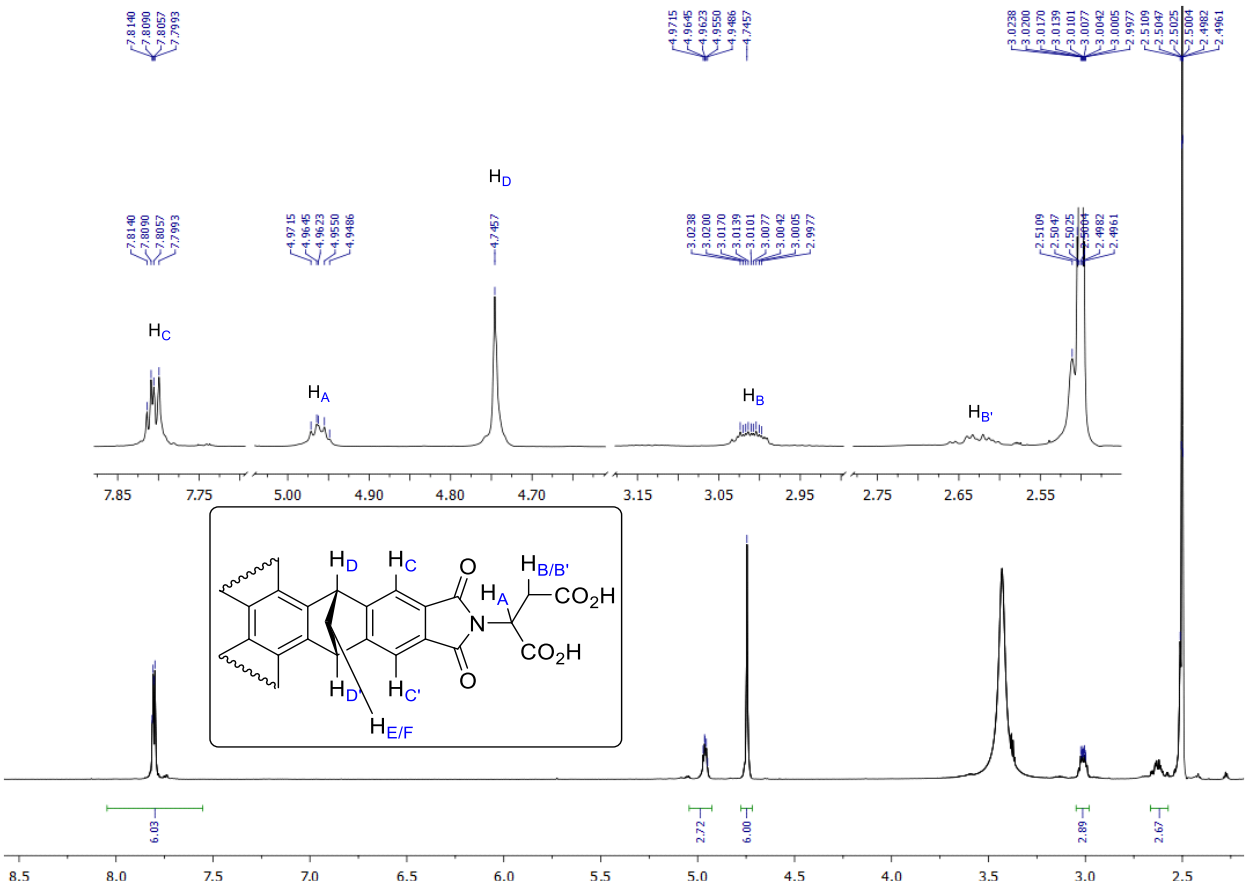

Figure S1. ^{1}H NMR spectrum (850 MHz, 298 K) of basket **1** in DMSO-*d*$_6$.

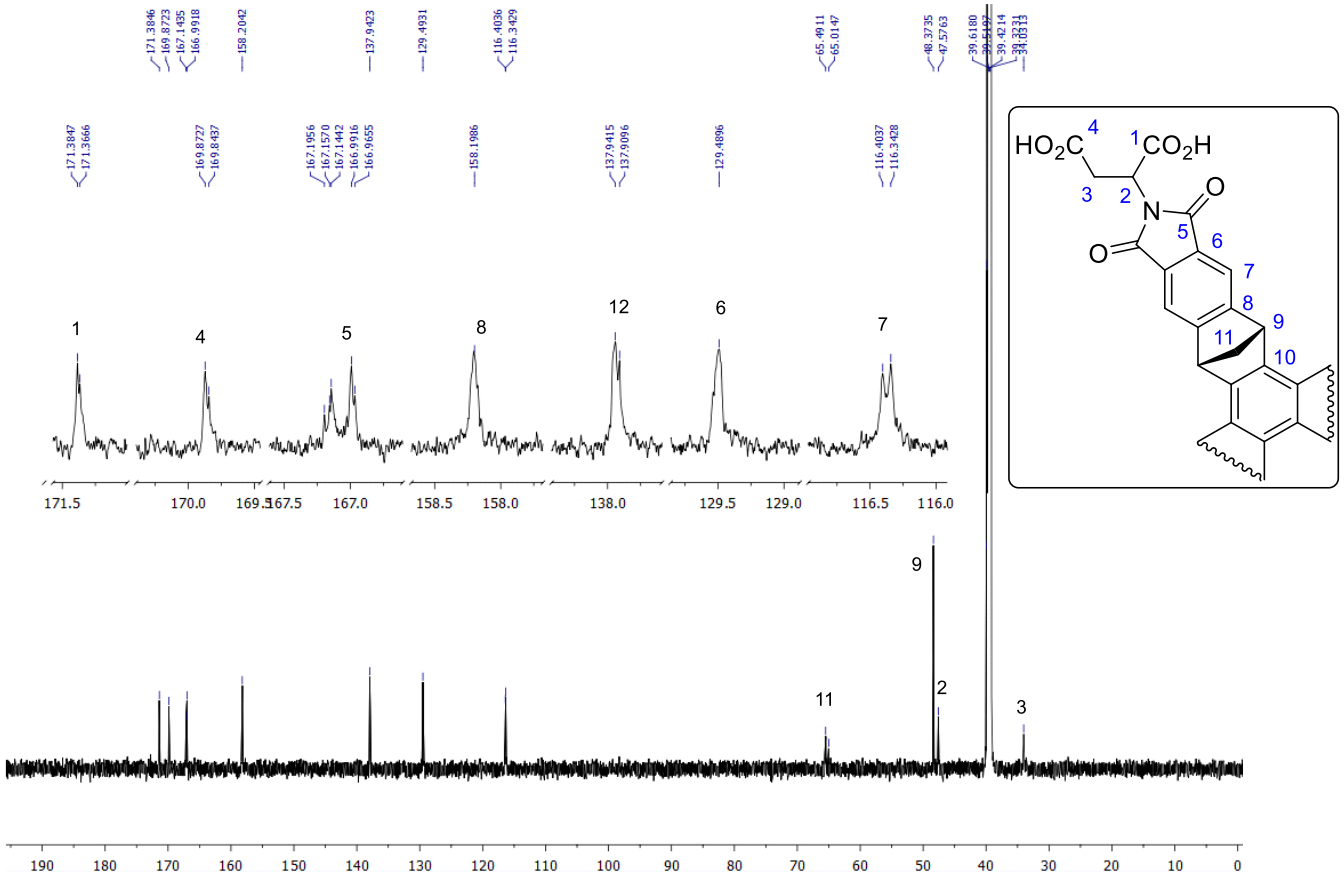

Figure S2. ^{13}C NMR spectrum (175 MHz, 298 K) of basket **1** in DMSO-d_6.

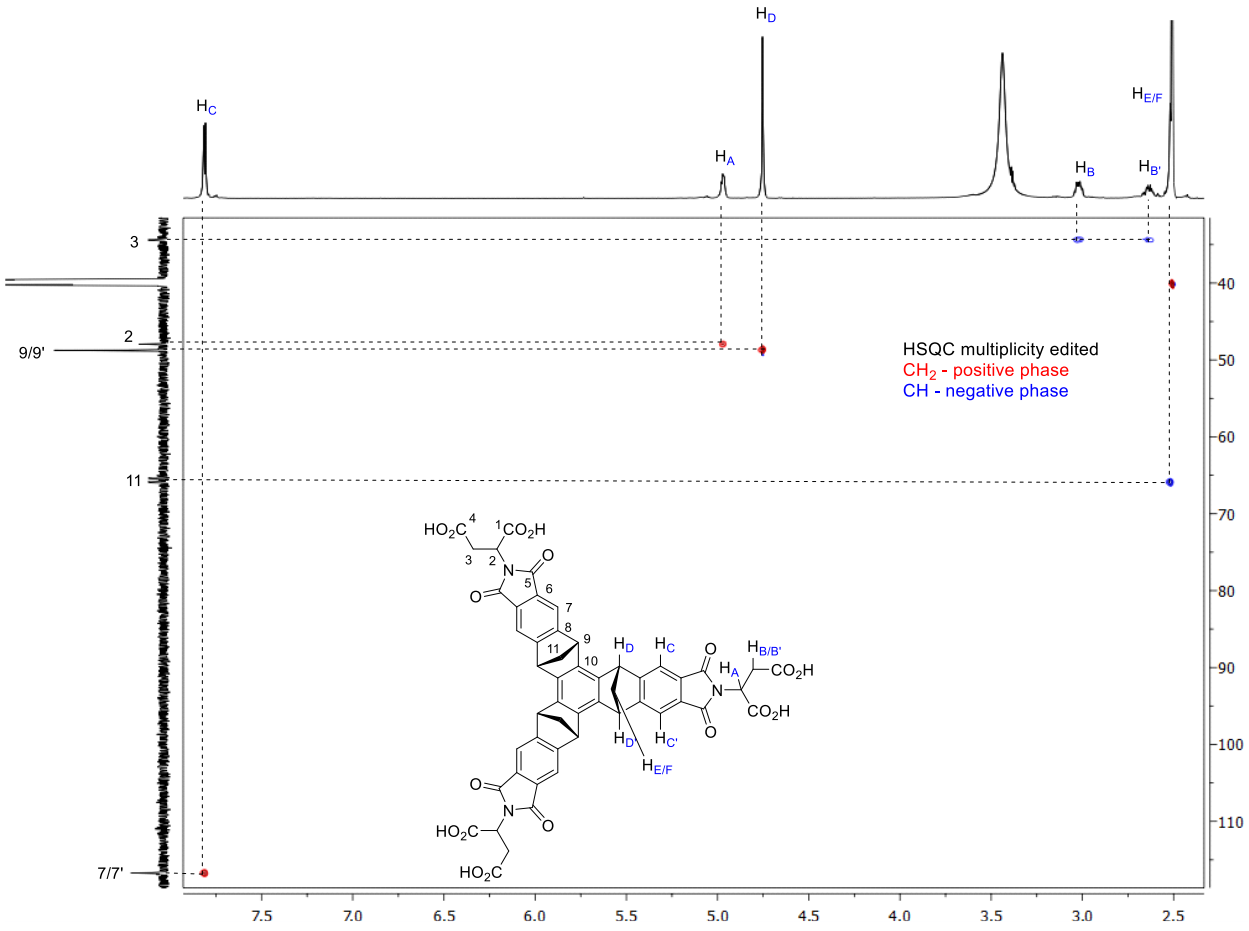

Figure S3. ^{1}H-^{13}C HSQC NMR spectrum (700 MHz, 298 K) of basket **1** in DMSO-d_6.

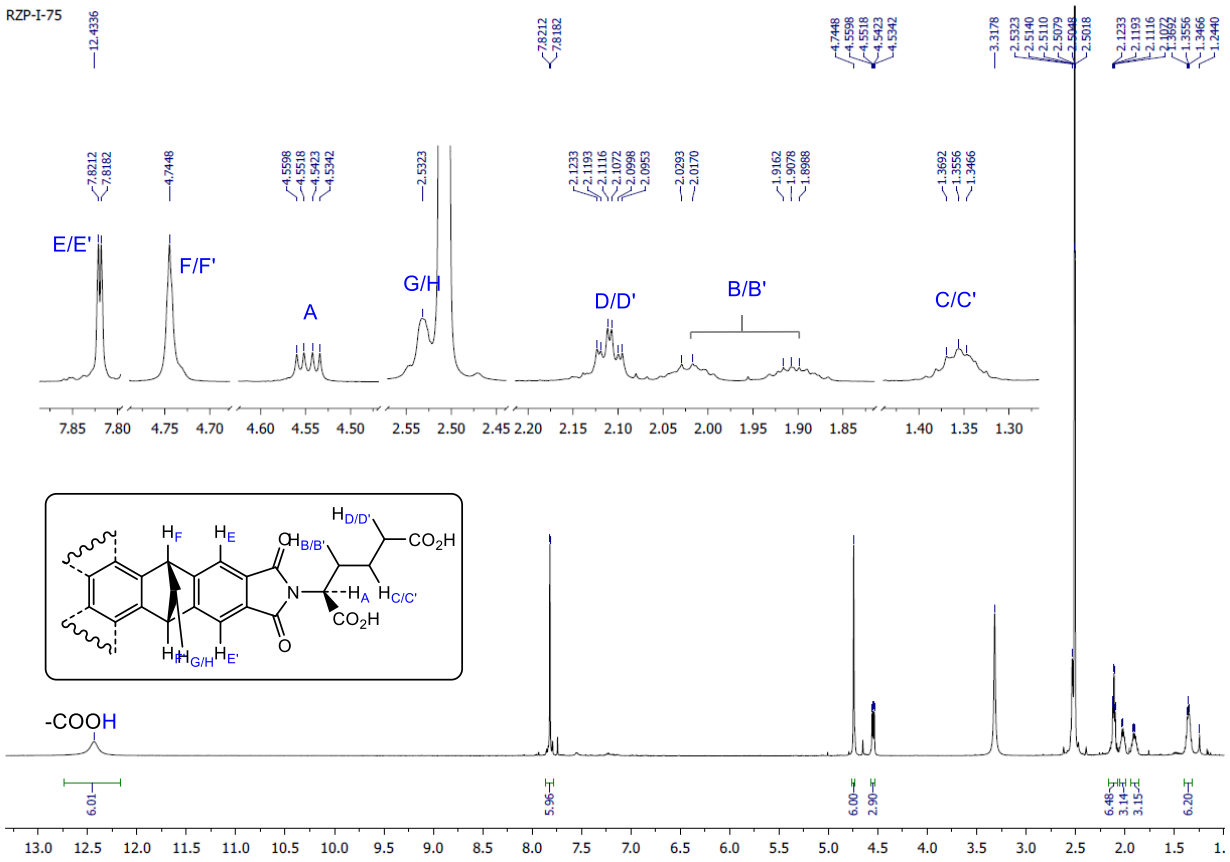

Figure S4. ^{1}H NMR spectrum (600 MHz, 298 K) of basket **3** in DMSO-d_6.

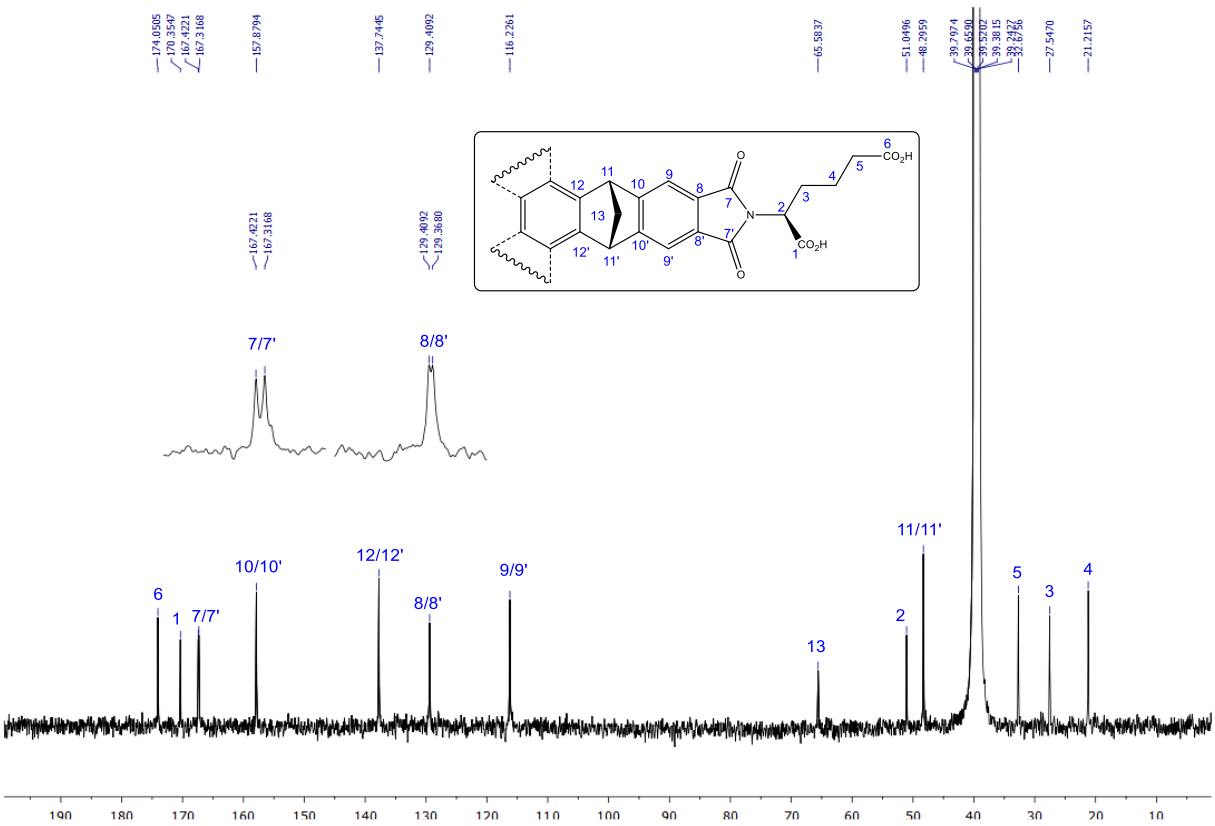

Figure S5. ^{13}C NMR (150 MHz, 298 K) of basket **3** in DMSO-d_6.

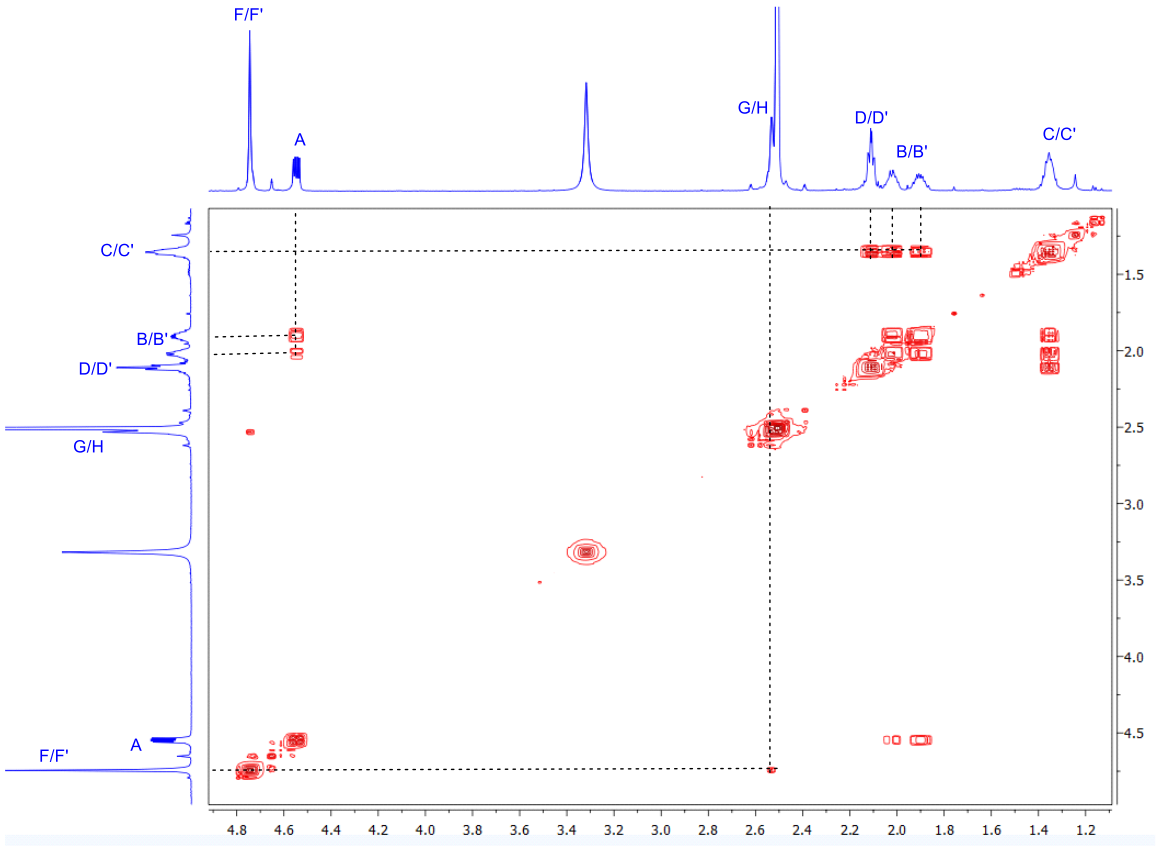

Figure S6. ^{1}H-^{1}H COSY NMR spectrum (600 MHz, 298 K) of basket **3** in DMSO-d_6.

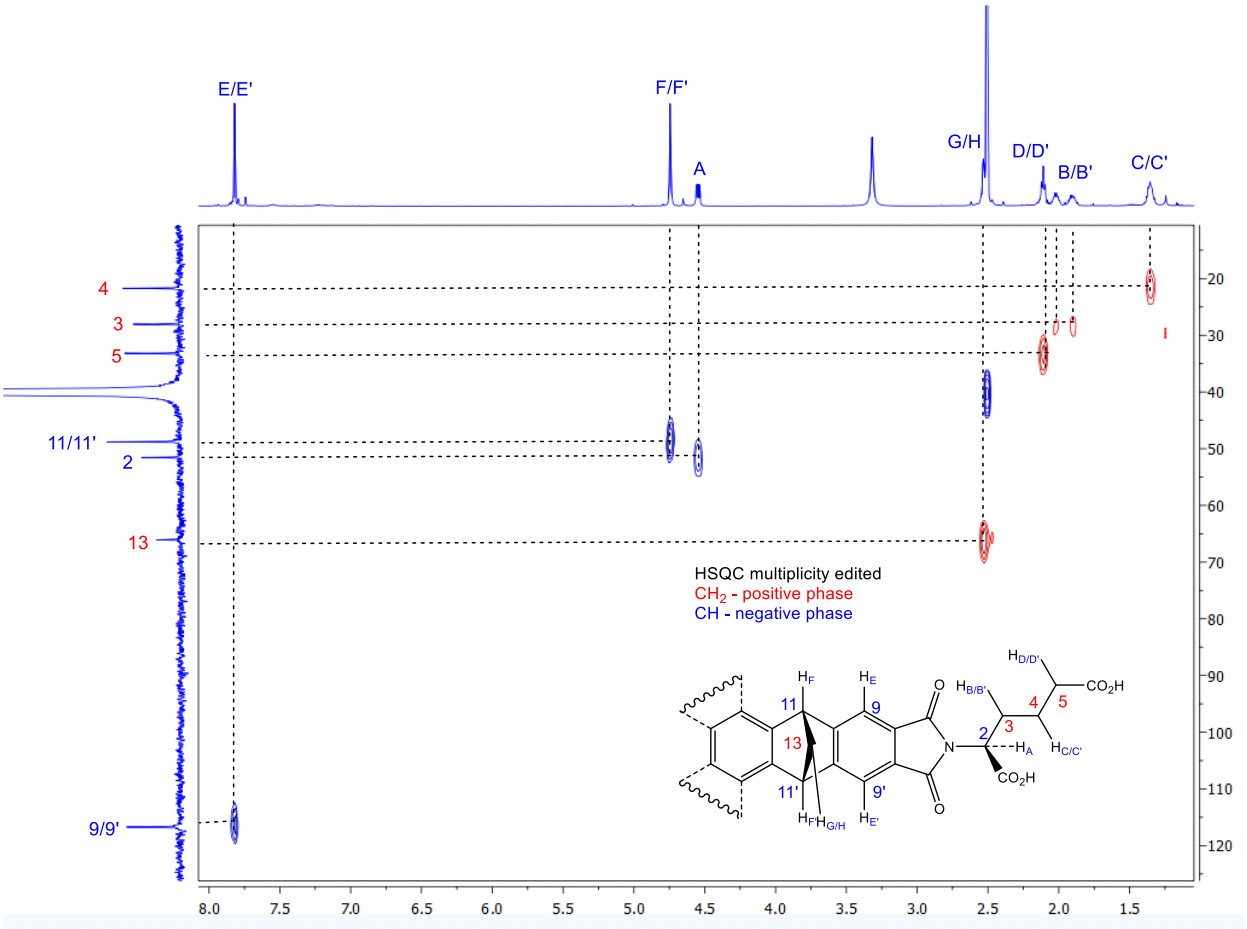

Figure S7. ^{1}H-^{13}C HSQC NMR spectrum (600 MHz, 298 K) of basket **3** in DMSO-d_6.

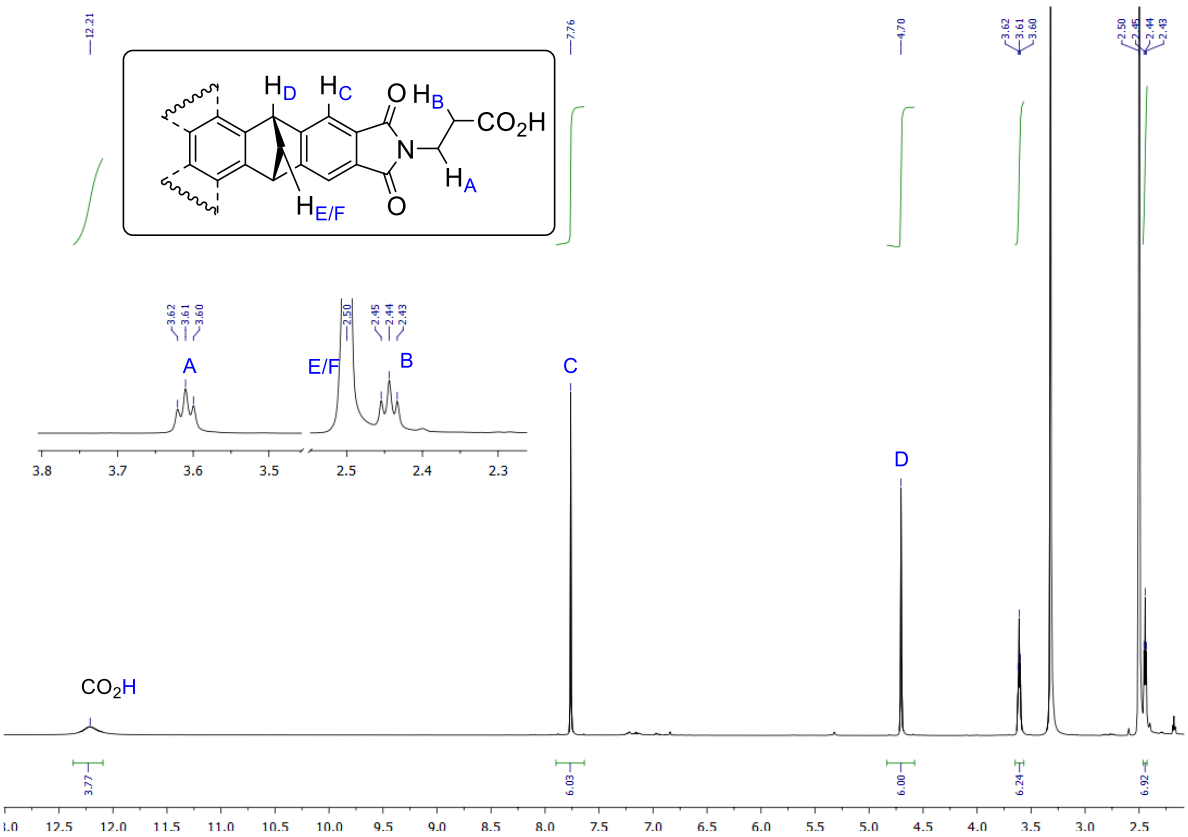

Figure S8. ^{1}H NMR spectrum (700 MHz, 298 K) of basket **4** in DMSO-d_6.

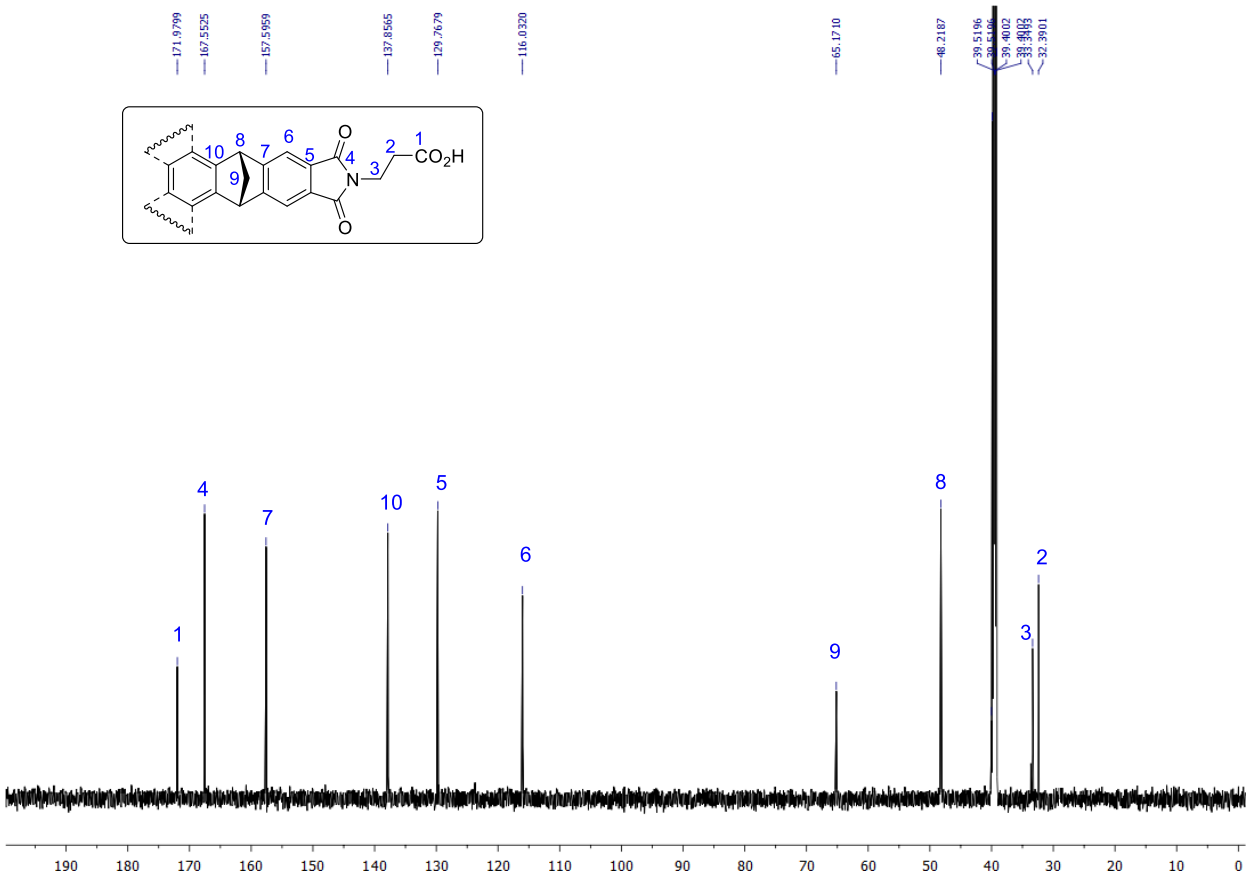

Figure S9. ^{13}C NMR (150 MHz, 298 K) of basket **4** in DMSO-d_6.

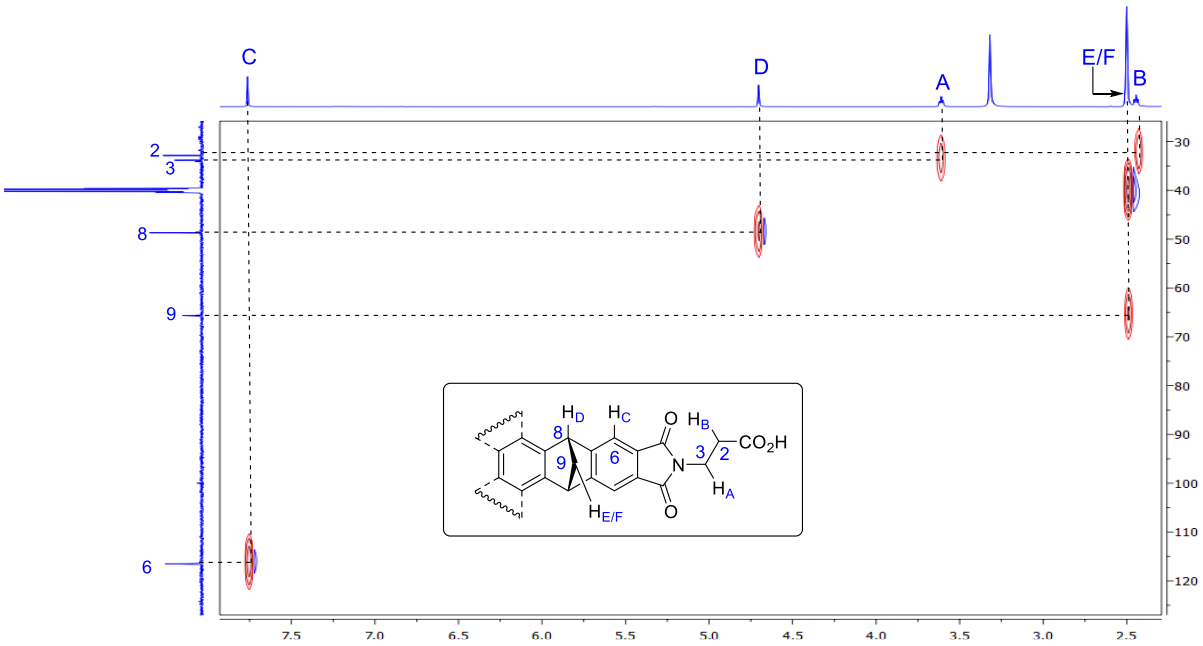

Figure S10. ^{1}H-^{13}C HSQC NMR spectrum (700 MHz, 298 K) of basket **4** in DMSO-d_6.

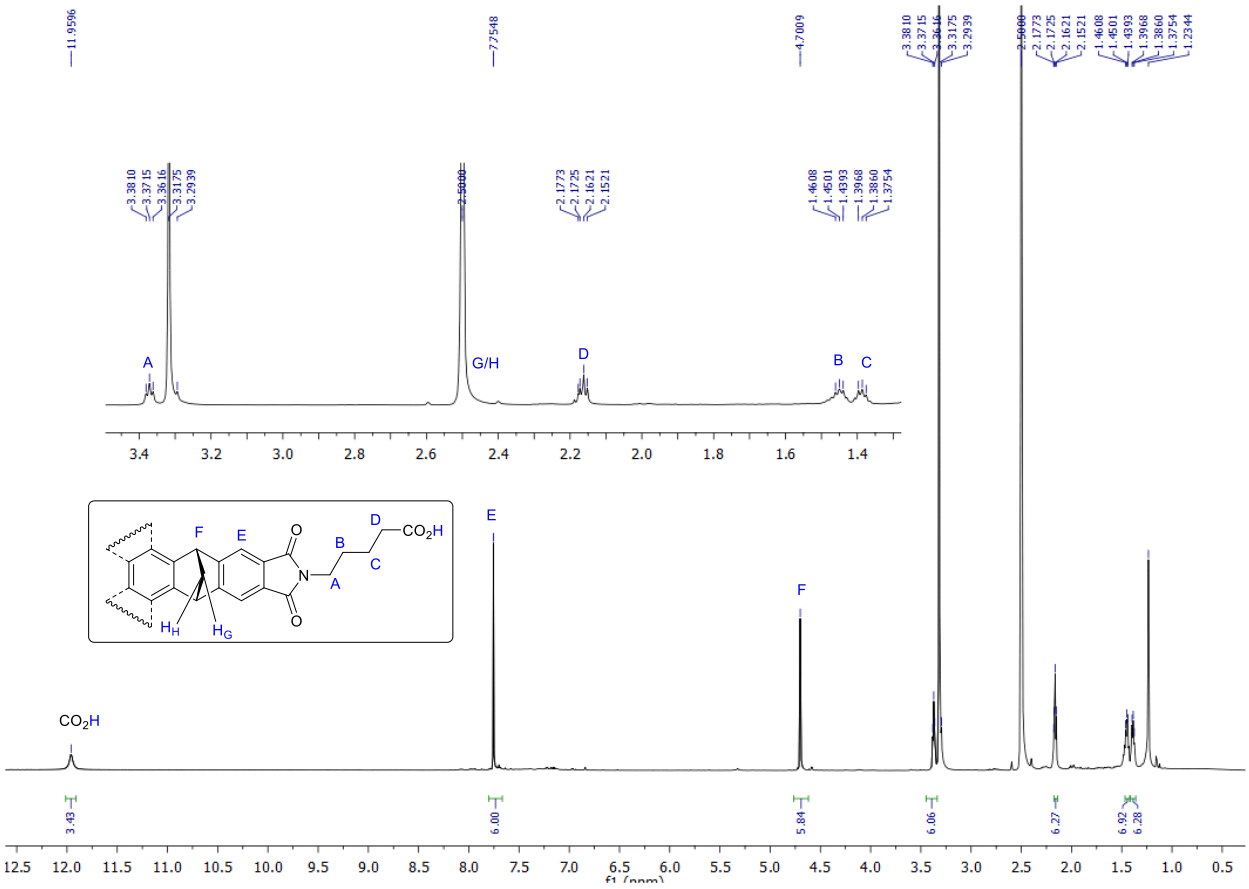

Figure S11. ^{1}H NMR spectrum (700 MHz, 298 K) of basket **6** in DMSO-d_6.

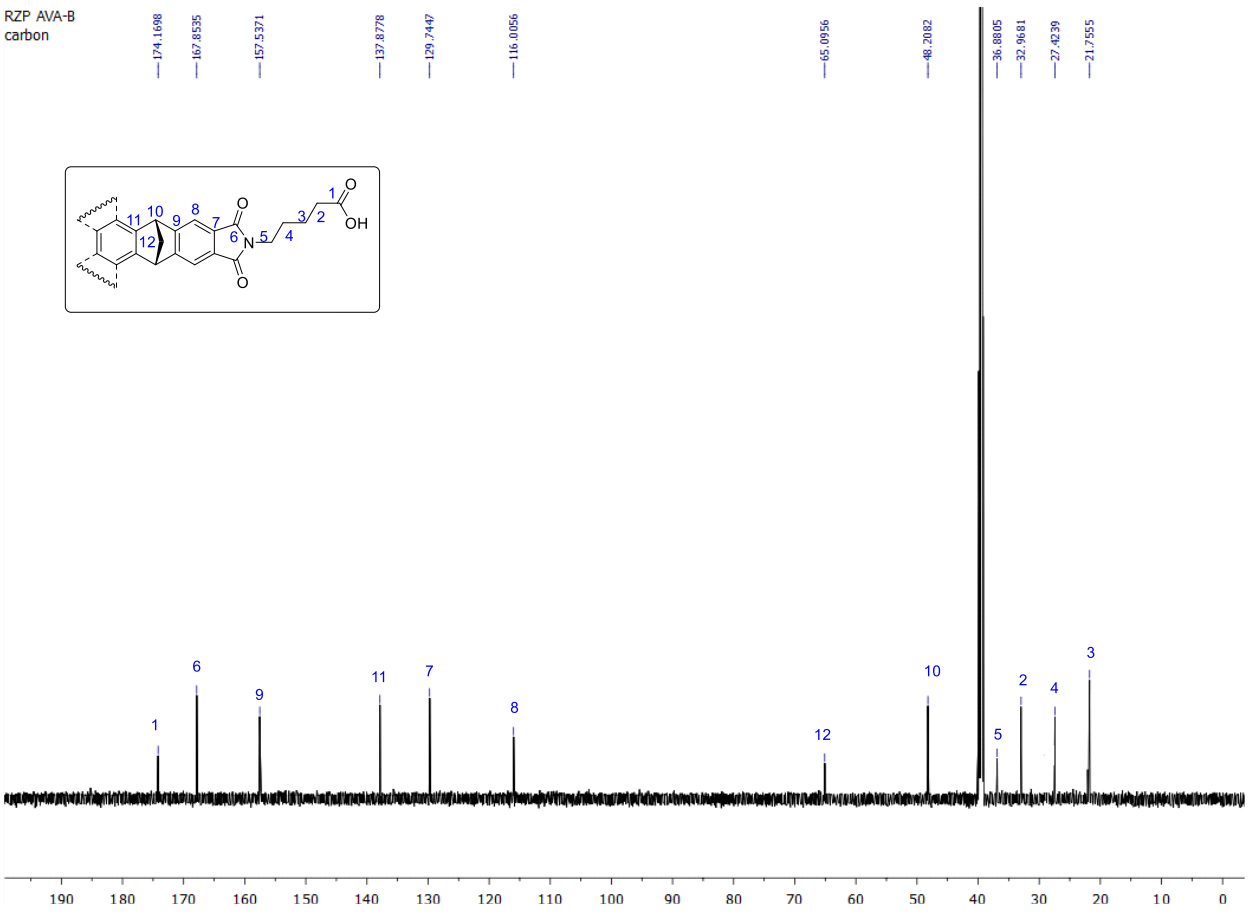

Figure S12. ^{13}C NMR (175 MHz, 298 K) of basket **6** in DMSO-d_6.

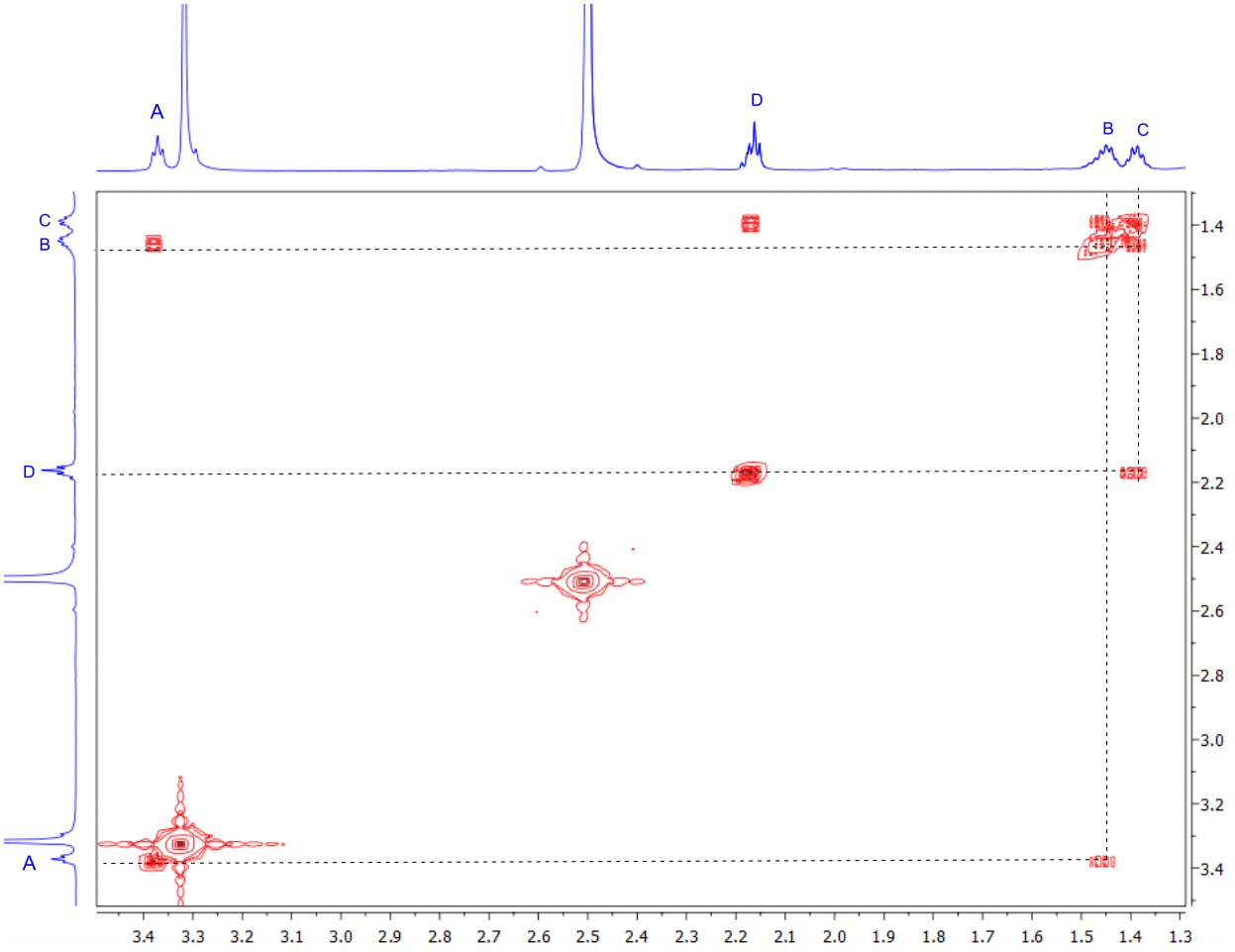

Figure S13. ^{1}H-^{1}H COSY NMR spectrum (700 MHz, 298 K) of basket **6** in DMSO-d_6.

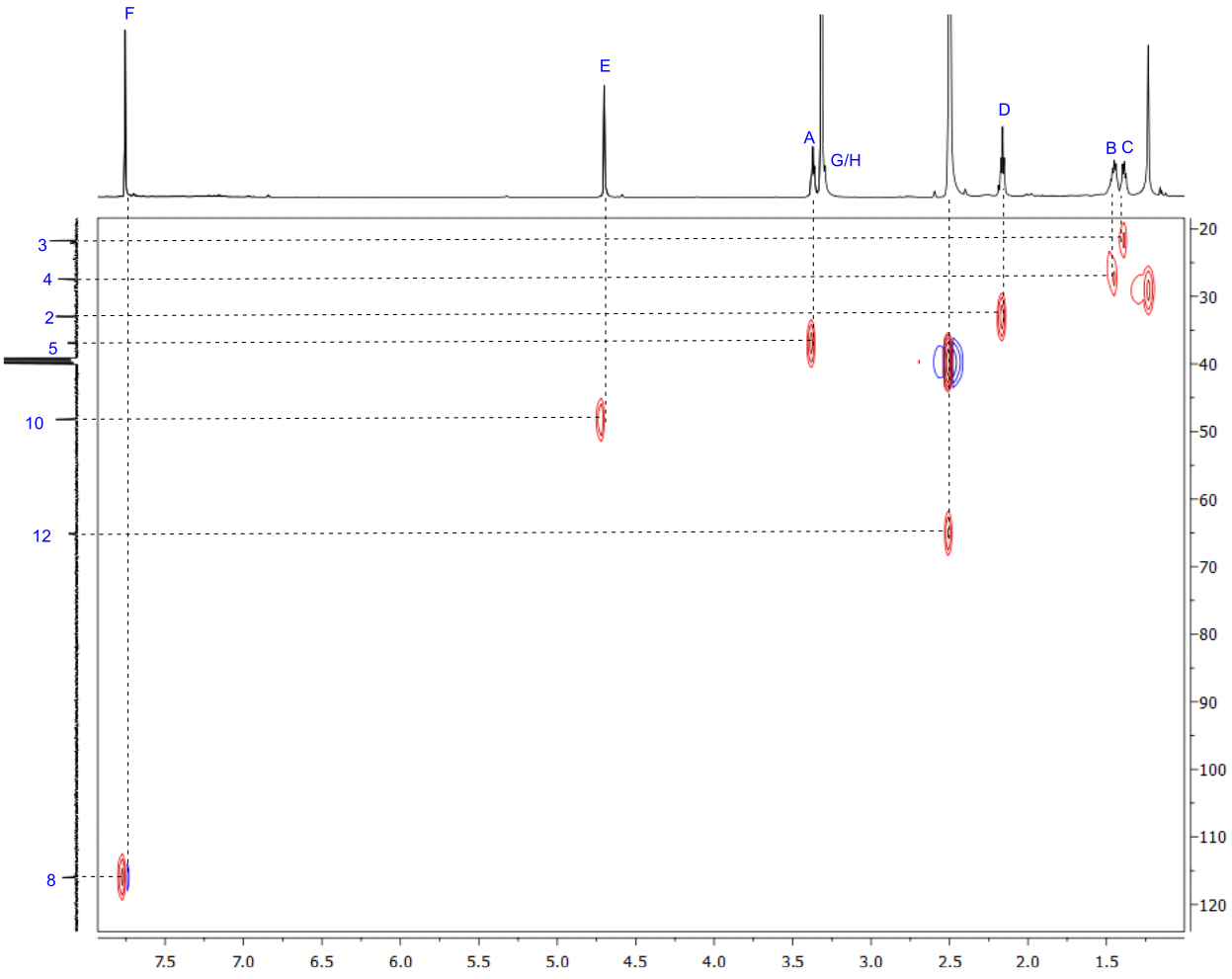

Figure S14. ^{1}H-^{13}C HSQC NMR spectrum (700 MHz, 298 K) of basket **6** in DMSO-d_6.

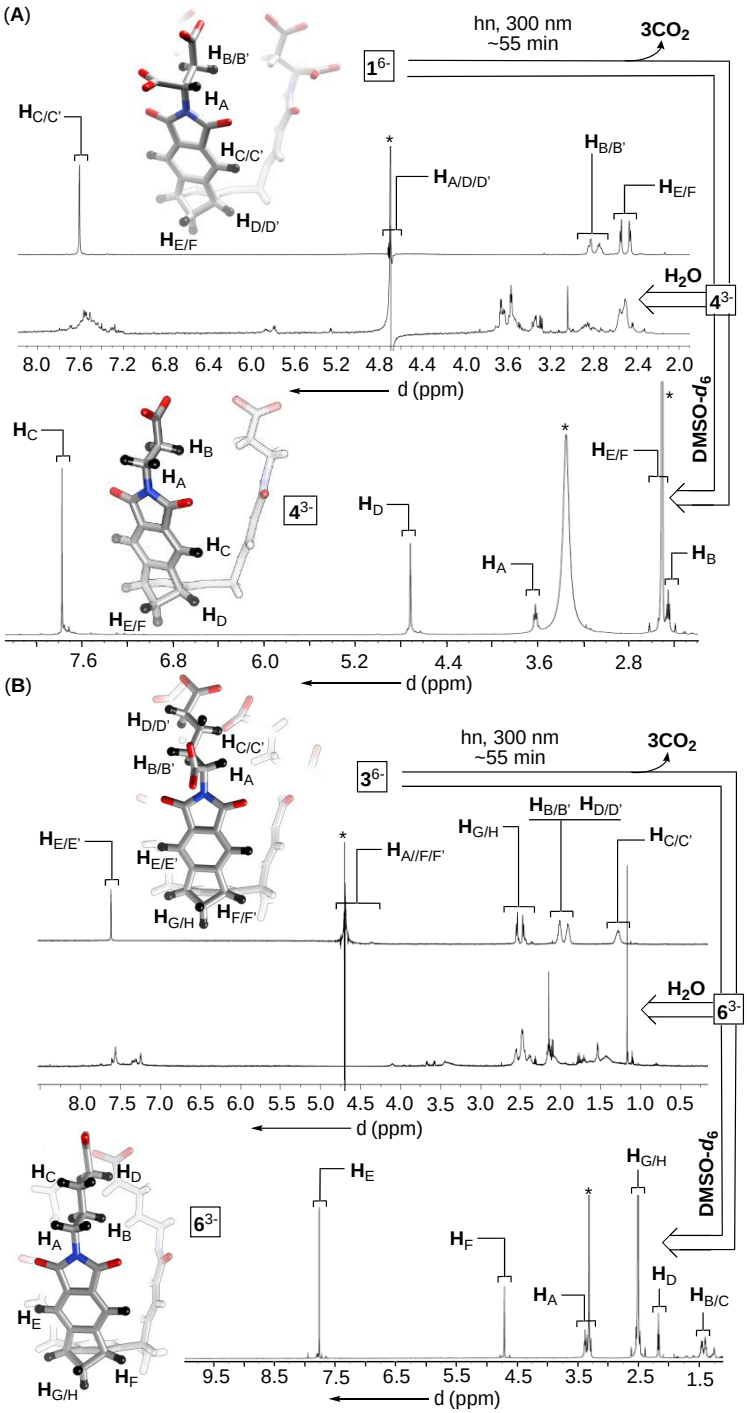

Figure S15. (A) ^{1}H NMR spectra (600 MHz, 298 K) of 0.1 mM solution of $\mathbf{1}^{6-}$ (30 mM phosphate buffer at pH = 7.0) before and after 300 nm irradiation (Rayonet) for 55 minutes. (Bottom) ^{1}H NMR spectrum (600 MHz, 298 K) of $\mathbf{4}^{3-}$ in DMSO-d_6. (B) ^{1}H NMR spectra (600 MHz, 298 K) of 0.1 mM solution of $\mathbf{3}^{6-}$ (30 mM phosphate buffer at pH = 7.0) before and after 300 nm irradiation (Rayonet) for 55 minutes. (Bottom) ^{1}H NMR spectrum (600 MHz, 298 K) of $\mathbf{6}^{3-}$ in DMSO-d_6.

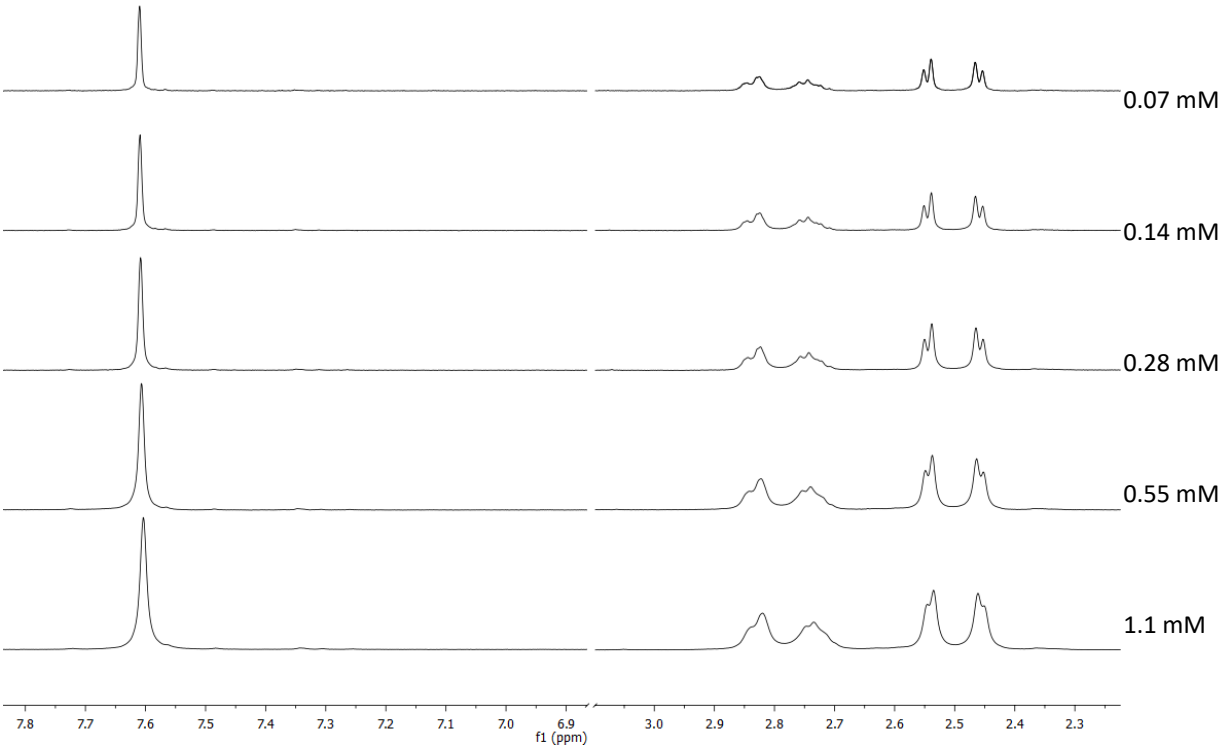

Figure S16. ^{1}H NMR spectra (600 MHz, 298.0 K) of basket $\mathbf{1^{6-}}$ (in 30.0 mM phosphate buffer with 20% D_2O at pH = 7.0 ± 0.1) obtained upon an incremental dilution; note that solution concentrations at which the spectra were taken are shown on the right.

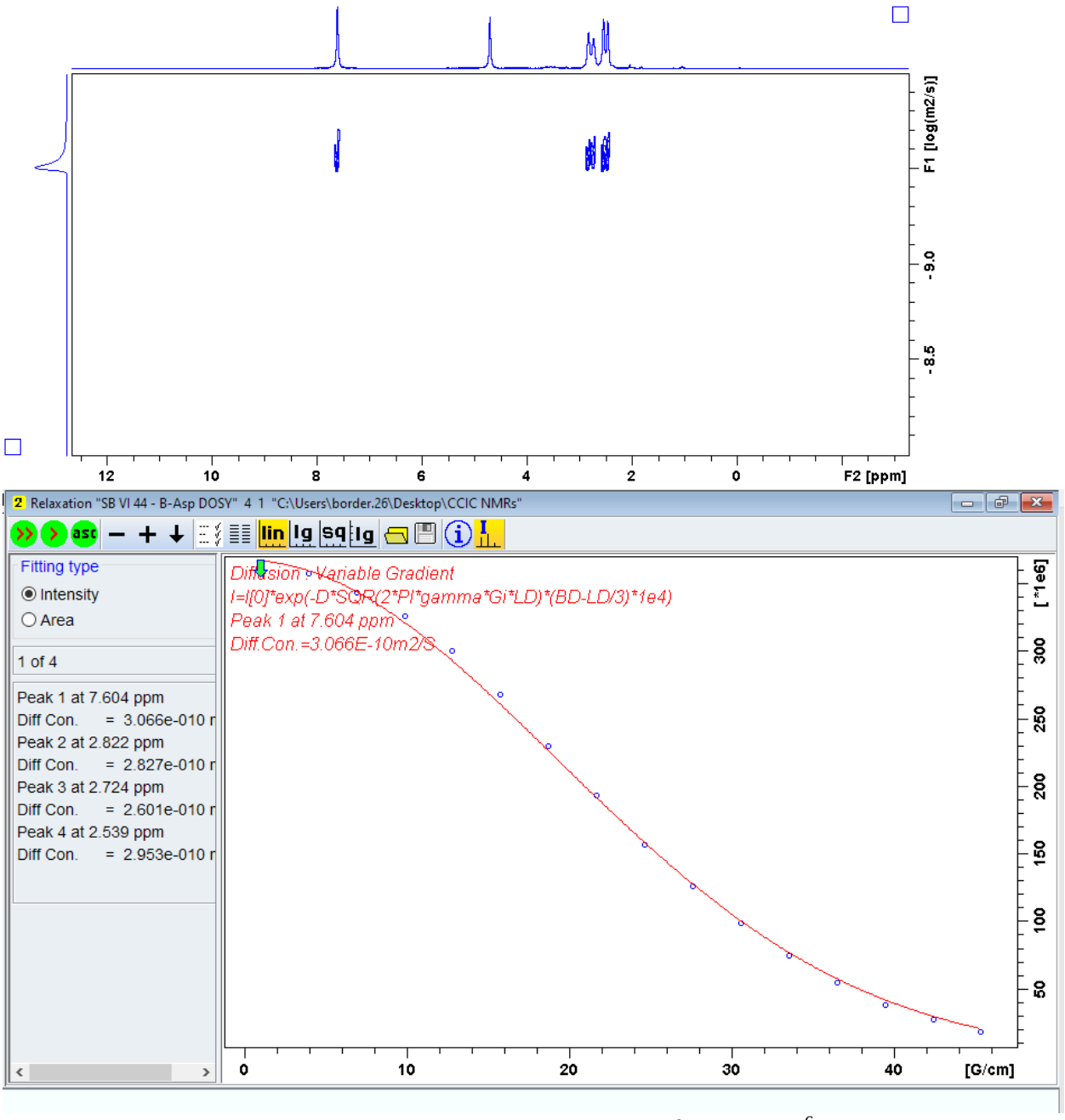

Figure S17. (Top) DOSY NMR spectrum (600 MHz, 298 K) of 0.5 mM $\mathbf{1}^{6-}$ in 30 mM phosphate buffer (H_2O:D_2O = 9:1) at pH = 7.0. (Bottom) The change in intensity of resonance corresponding to $H_{B/B'}$ proton as a function of the field gradient g (G/cm) was obtained using the pulse field gradient stimulated echo sequence with bipolar gradient pulse pair, 1 spoil gradient, 3-9-19 WATERGATE solvent suppression (stebpgp1s19) pulse sequence and the data was fit to the Stejskal-Tanner equation to give the value of diffusion coefficient D (m^2/s); the process was completed for resonances $H_{B/B'}$, H_C, H_F and H_G and the reported value of D is the arithmetic mean of 4 numerical values. The hydrodynamic radius was computed using the Stokes-Einstein equation whereby the viscosity of 30.0 mM phosphate buffer at pH = 7.0 ± 0.1 is assumed to be similar to that of H_2O:D_2O = 9:1 (η = 0.91 mPa s at 298.1).

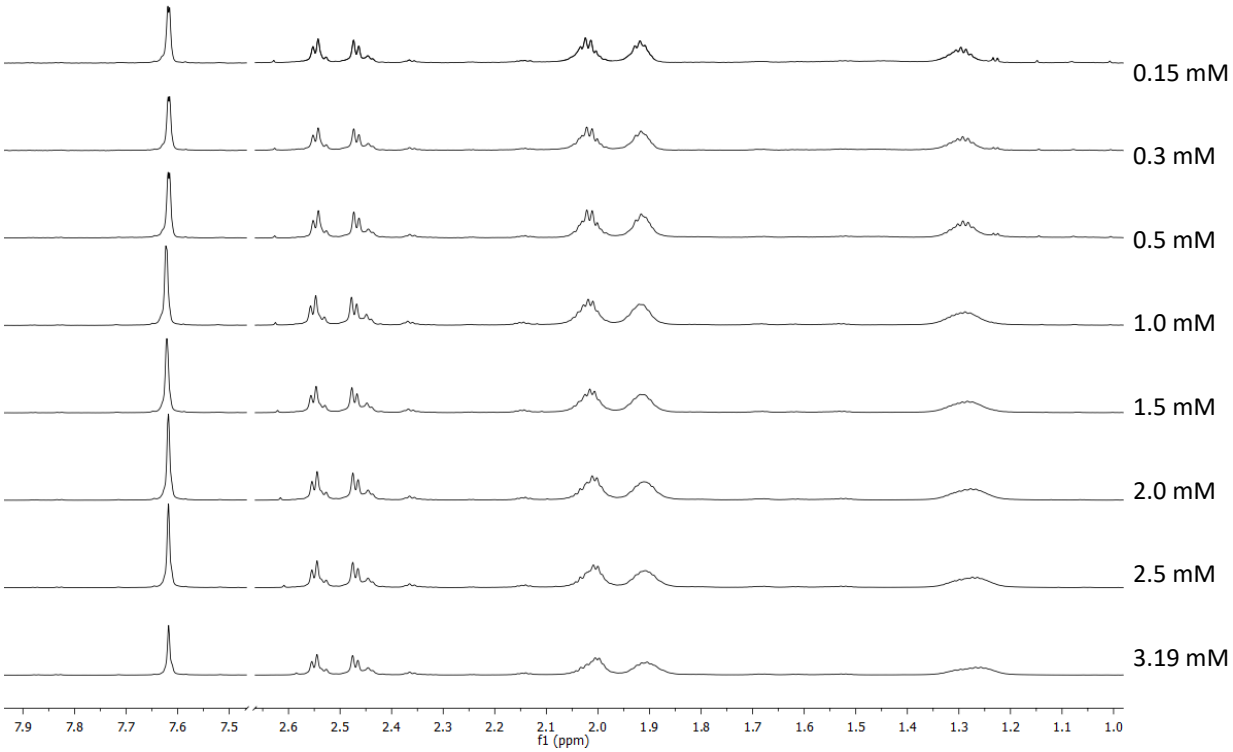

Figure S18. ^{1}H NMR spectra (600 MHz, 298.0 K) of basket $\mathbf{3}^{6-}$ (in 30.0 mM phosphate buffer with 20% D_2O at pH = 7.0 ± 0.1) obtained upon an incremental dilution; note solution concentrations at which the spectra were taken are shown on the left.

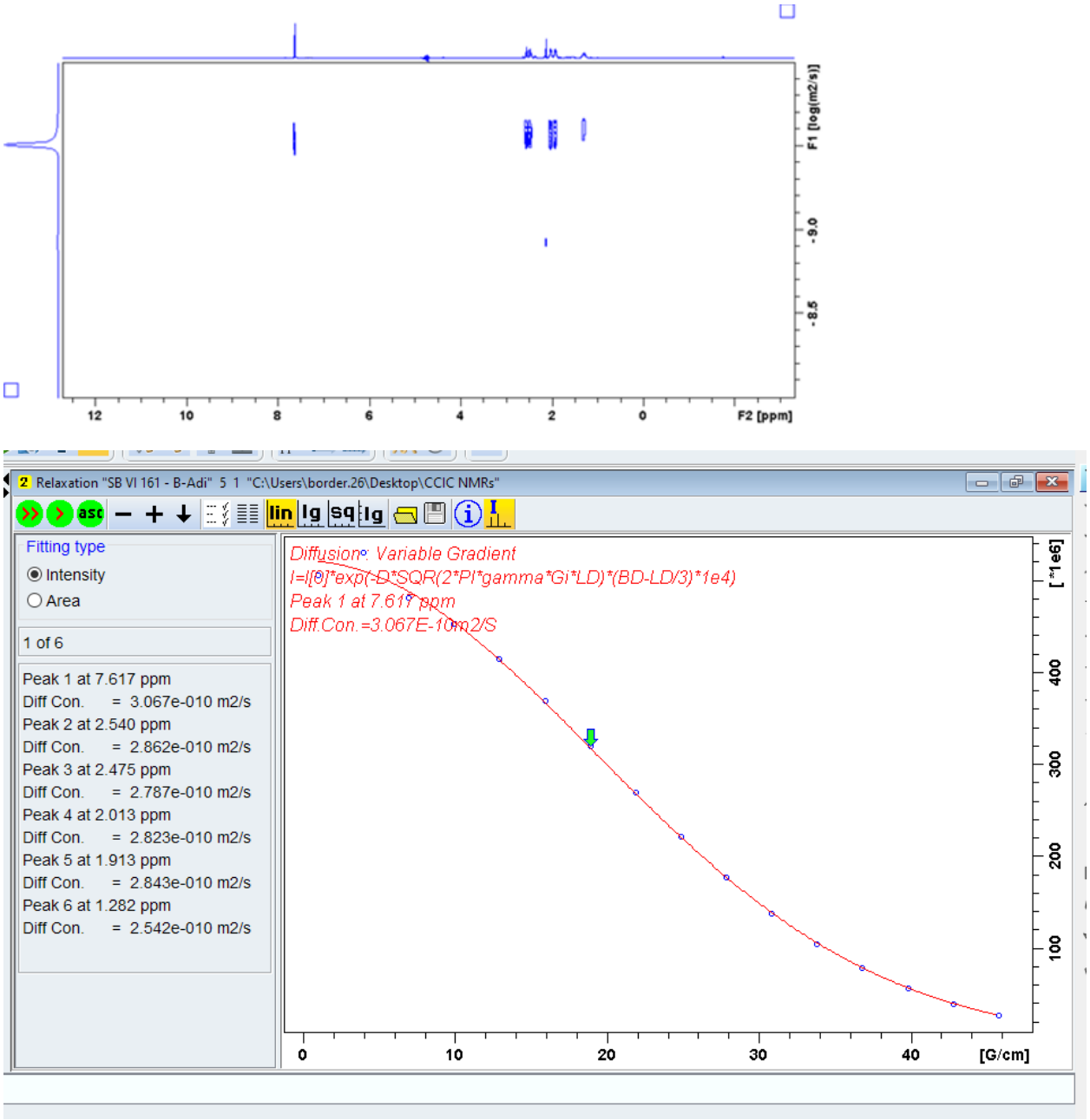

Figure S19. (Top) DOSY NMR spectrum (600 MHz, 298 K) of 0.3 mM $\mathbf{3}^{6-}$ in 30 mM phosphate buffer (H_2O:D_2O = 9:1) at pH = 7.0. (Bottom) The change in intensity of resonance corresponding to $H_{A/A'}$ proton as a function of the field gradient *g* (G/cm) was obtained using the pulse field gradient stimulated echo sequence with bipolar gradient pulse pair, 1 spoil gradient, 3-9-19 WATERGATE solvent suppression (stebpgp1s19) pulse sequence and the data was fit to the Stejskal-Tanner equation to give the value of diffusion coefficient *D* (m^2/s); the process was completed for resonances $H_{B/B'}$, $H_{C/C'}$, $H_{D/D'}$, $H_{E/E'}$, H_H, H_G and the reported value of *D* is the arithmetic mean of 6 numerical values. The hydrodynamic radius was computed using the Stokes-Einstein equation whereby the viscosity of 30.0 mM phosphate buffer at pH = 7.0 ± 0.1 is assumed to be similar to that of H_2O:D_2O = 9:1 (η = 0.91 mPa s at 298.1). Note that signal at 2.1 ppm corresponds to residual acetic acid.

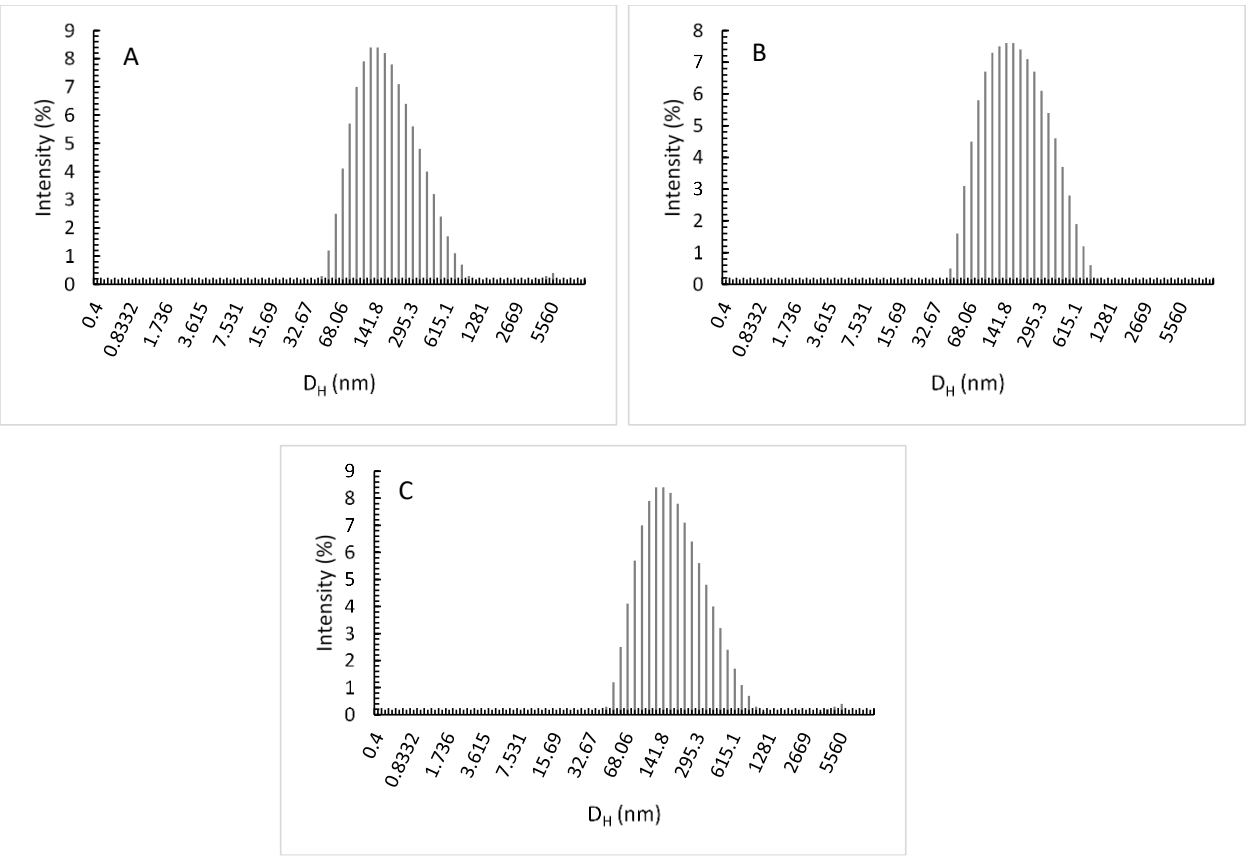

Figure S20. The intensity distribution of scattered light as a function of hydrodynamic radii (D_H) particle size was obtained from Dynamic Light Scattering (DLS, 298 K) measurements of 1.0 mM solution of $\mathbf{3}^{6-}$ in 30.0 mM phosphate buffer at pH = 7.0 ± 0.1; DLS data were analyzed using the viscosity of 0.8872 cP and refractive index (RI) = 1.330 (from pure water). (A) D_H = 217.8 nm, DCR = 6471.8 kcps, PDI = 0.262. (B) D_H = 204.1 nm, DCR = 6277.8 kcps, PDI = 0.254. (C) D_H = 213.8 nm, DCR = 6241.7 kcps, PDI = 0.266. The reported value of D_H = 212 ± 7 nm is an arithmetic mean of three measurements with the standard deviation as the error.

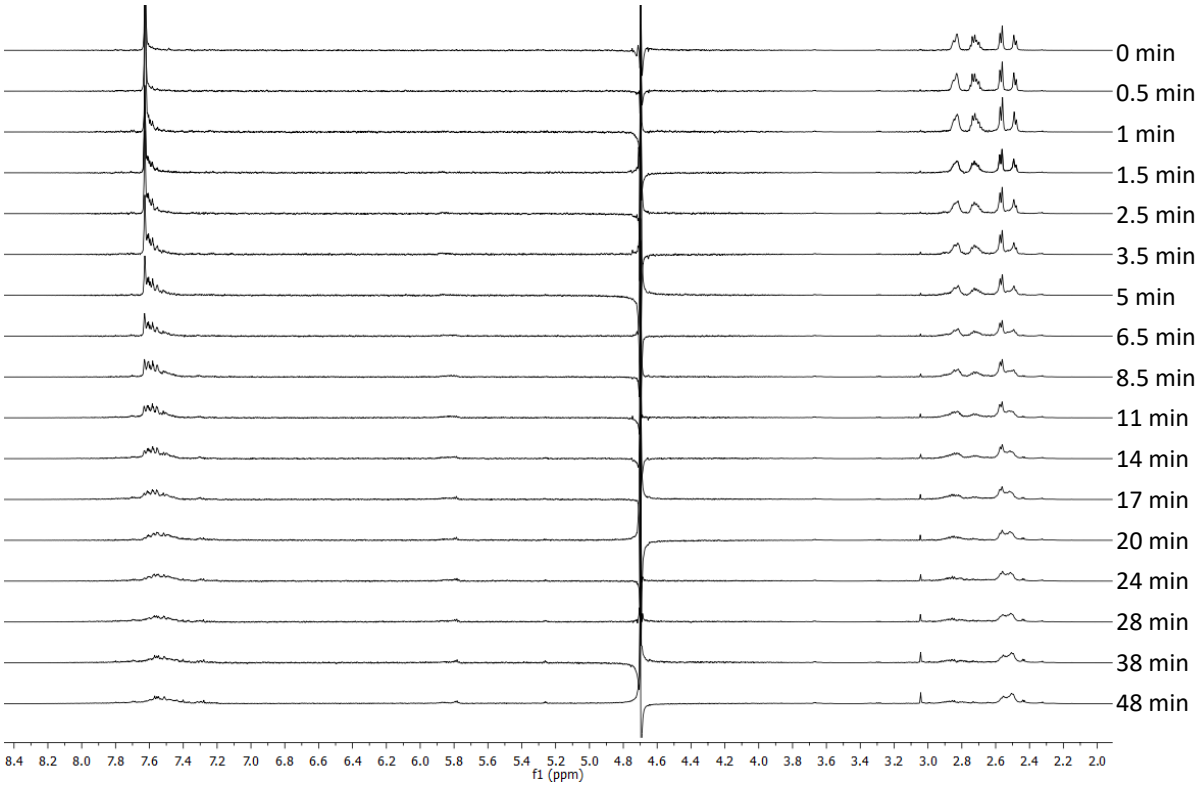

Figure S21. ^{1}H NMR spectra (700 MHz, 298.0 K) of 0.1 mM solution of $\mathbf{1}^{6-}$ (30.0 mM phosphate buffer at pH = 7.0 ± 0.1) obtained upon irradiation (Rayonet) at 300 nm; note that times at which the spectra were taken are shown on the right. A standard solution of $\mathbf{1}^{6-}$ was prepared in 30.0 mM phosphate buffer (containing 20% of D_2O) at pH 7.0 ± 0.1; the pH of the solution was adjusted to 7.0 using 0.3 M NaOH. 500 µL of this solution, contained in an NMR tube, was placed inside a Rayonet reactor at temperature of 35˚C (fan). The samples were irradiated at 300 nm (sixteen 3000Å bulbs distributed symmetrically around the chamber). At the above specified time intervals, we would remove the NMR tube from the reactor to record ^{1}H NMR spectrum (water suppression NMR pulse sequence for saturating the signal of the solvent).

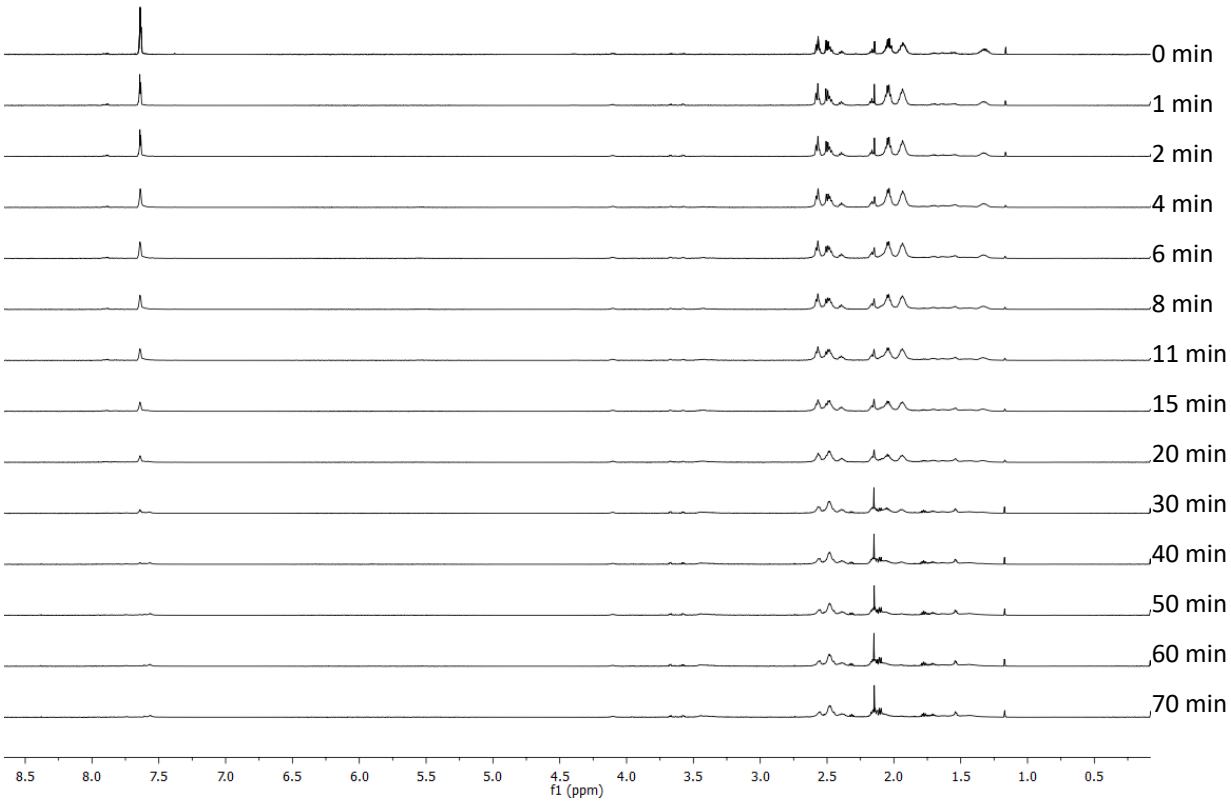

Figure S22. ^{1}H NMR spectra (700 MHz, 298.0 K) of 0.1 mM solution of $\mathbf{3}^{6-}$ (30.0 mM phosphate buffer at pH = 7.0 ± 0.1) obtained upon irradiation (Rayonet) at 300 nm; note that times at which the spectra were taken are shown on the right. A standard solution of $\mathbf{3}^{6-}$ was prepared in 30.0 mM phosphate buffer (containing 20% of D_2O) at pH 7.0 ± 0.1; the pH of the solution was adjusted to 7.0 using 0.3 M NaOH. 500 µL of this solution, contained in an NMR tube, was placed inside a Rayonet reactor at temperature of 35˚C (fan). The samples were irradiated at 300 nm (sixteen 3000Å bulbs distributed symmetrically around the chamber). At the above specified time intervals, we would remove the NMR tube from the reactor to record ^{1}H NMR spectrum (water suppression NMR pulse sequence for saturating the signal of the solvent).

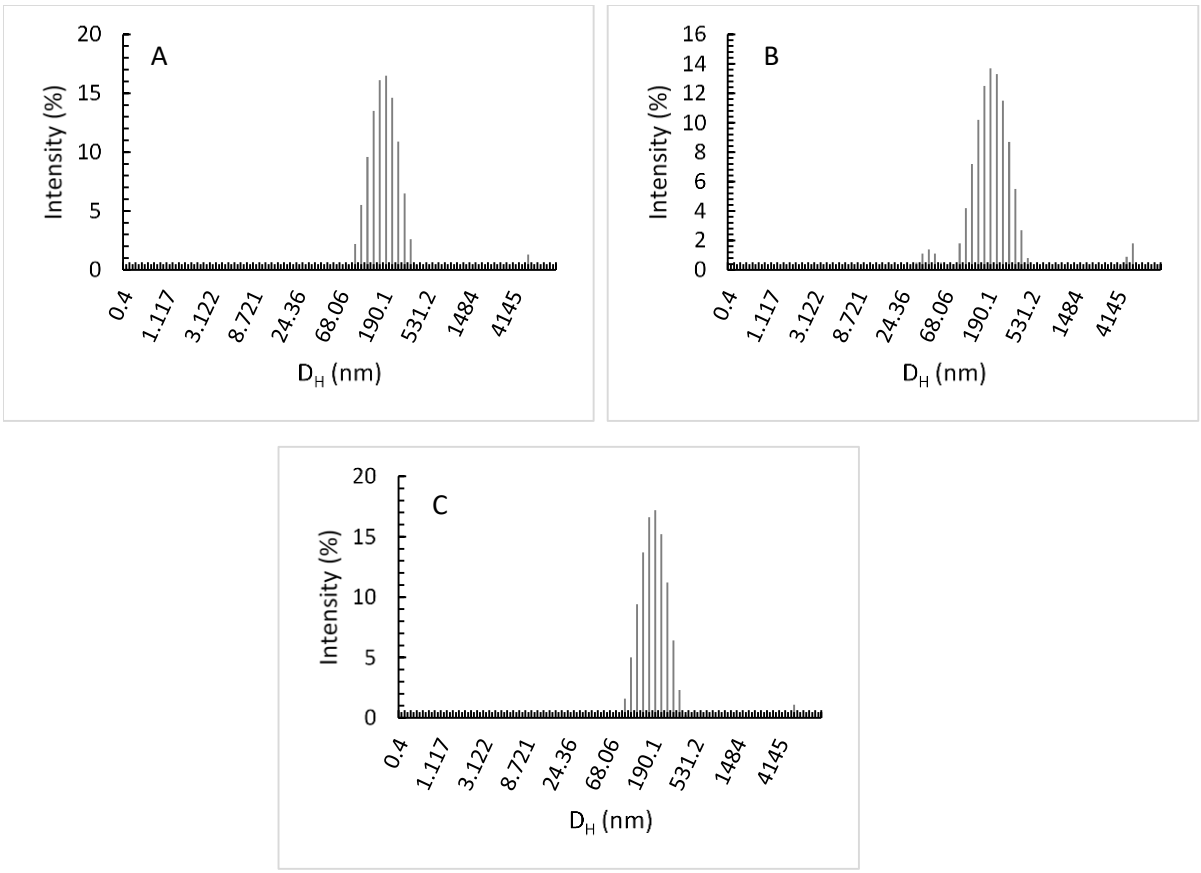

Figure S23. The intensity distribution of scattered light as a function of hydrodynamic radii (D_H) was obtained from Dynamic Light Scattering (DLS, 298 K) measurements of 1.0 mM solution of $\mathbf{4^{3-}}$ in 30.0 mM phosphate buffer at pH = 7.0 ± 0.1; DLS data were analyzed using the viscosity of 0.8872 cP and refractive index (RI) = 1.330 (from pure water). (A) D_H = 188.7 nm, DCR = 4056.7 kcps, PDI = 0.37. (B) D_H = 209.3 nm, DCR = 4239.2 kcps, PDI = 0.30. (C) D_H = 189.5 nm, DCR = 4368.5 kcps, PDI = 0.38. The reported value of D_H = 195 ± 12 nm is an arithmetic mean of three measurements with the standard deviation as the error.

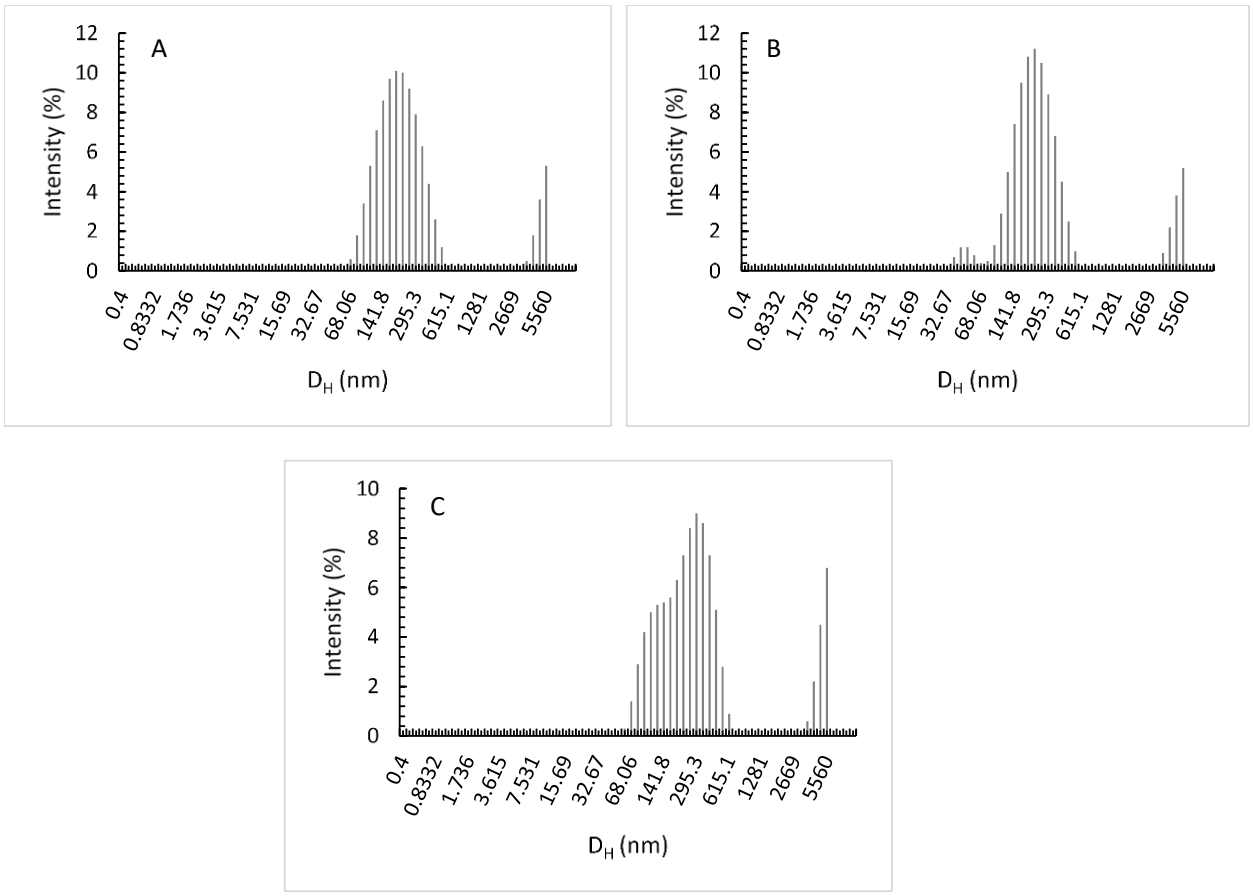

Figure S24. The intensity distribution of scattered light as a function of the particle size was obtained from Dynamic Light Scattering (DLS, 298 K) measurements of 1.0 mM solution of $\mathbf{6}^{3-}$ in 30.0 mM phosphate buffer at pH = 7.0 ± 0.1; DLS data were analyzed using the viscosity of 0.8872 cP and refractive index (RI) = 1.330 (from pure water). (A) average diameter = 219.7 nm, DCR = 1895.1 kcps, PDI = 0.55. (B) average diameter = 233.6 nm, DCR = 2066.2 kcps, PDI = 0.54. (C) average diameter = 249.5 nm, DCR = 2222.1 kcps, PDI = 0.57. The reported value of D_H = 235 ± 15 nm is an arithmetic mean of three measurements with the standard deviation as the error.

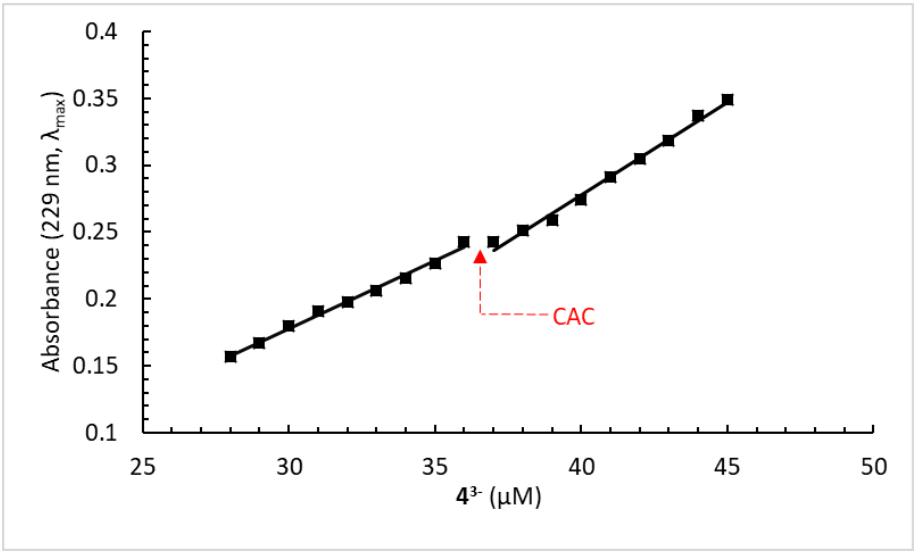

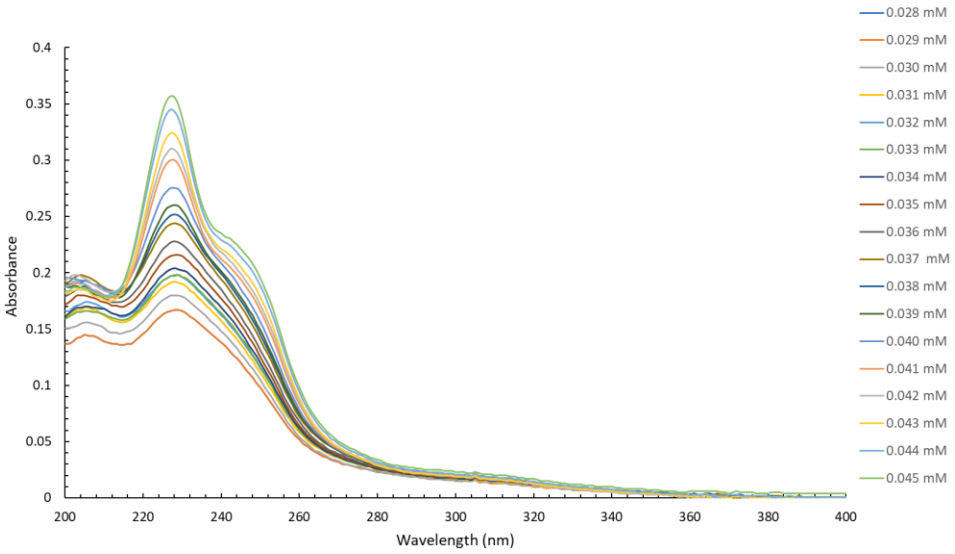

Figure S25. A standard 45 μM solution of $\mathbf{4}^{3-}$ in 30 mM phosphate buffer at pH = 7.0 ± 0.1 was sequentially diluted and monitored via UV-Vis spectroscopy. Between each point the solution contained in the cuvette was sonicated for 15 min. The path length of incident light was 5 mm. (Top) Plot of absorbance at 229 nm (λ_{max}) as a function of concentration. Each data set was fit to a linear function using excel with $R^2 > 0.99$. (Bottom) UV-vis spectra of variously concentrated $\mathbf{4}^{3-}$ (concentrations are shown on the right side).

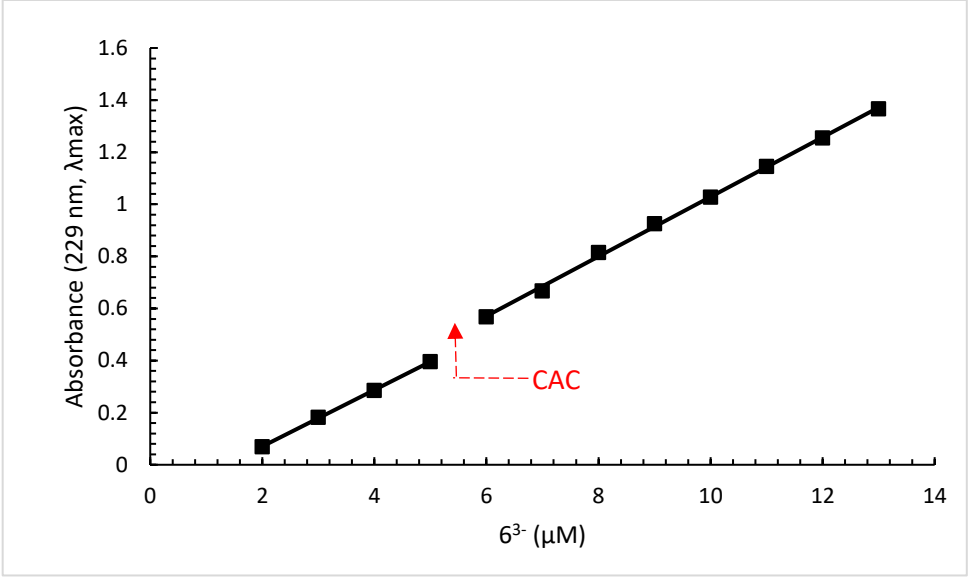

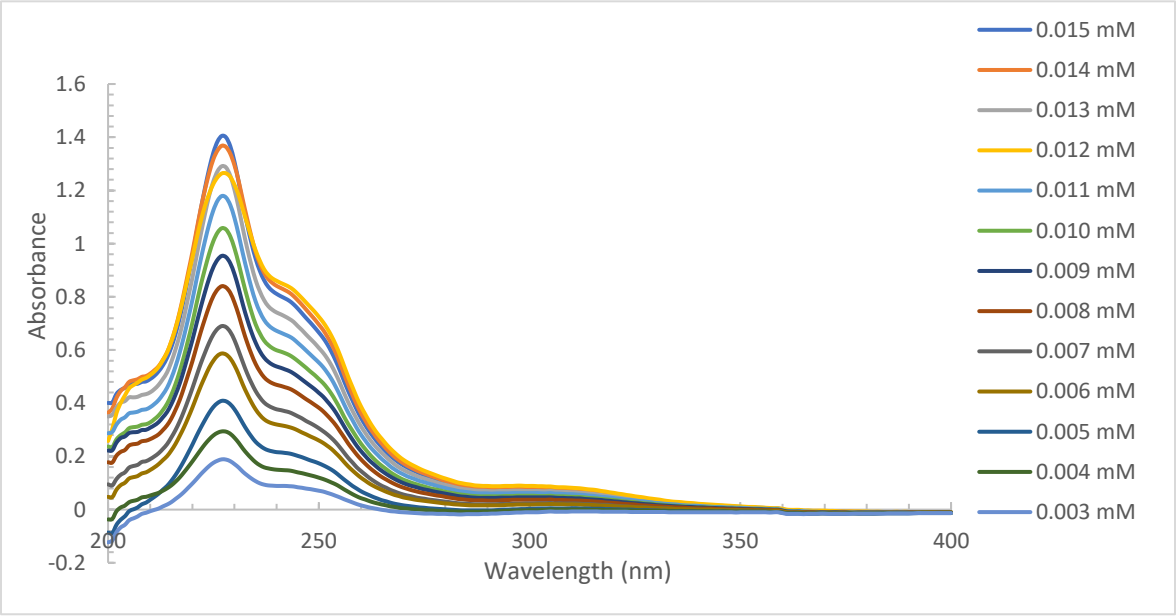

Figure S26. A standard 15 μM solution of $\mathbf{6^{3-}}$ in 30 mM phosphate buffer at pH = 7.0 ± 0.1 was sequentially diluted and monitored via UV-Vis spectroscopy to determine the critical aggregation concentration. The path length of incident light was 1 cm. (Top) Plot of absorbance at 229 nm (λ_{max}) as a function of concentration. Each data set was fit to a linear function using excel with $R^2 > 0.99$. (Bottom). UV-vis spectra of variously concentrated $\mathbf{6^{3-}}$ (concentrations are shown on the right side).

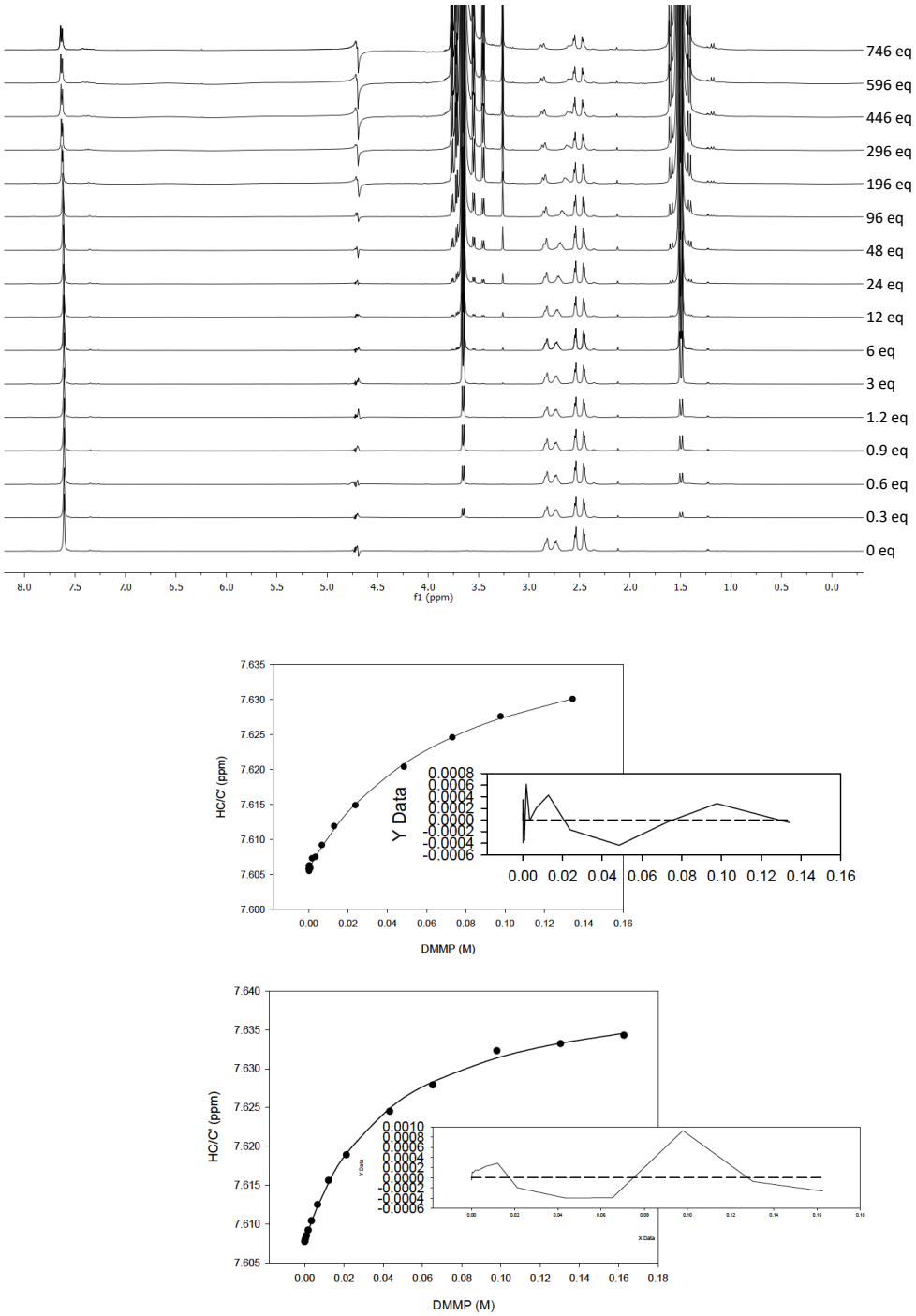

Figure S27. (Top) ^{1}H NMR spectra (700 MHz, 298 K) of 0.3 mM basket $\mathbf{1}^{6-}$ obtained upon incremental addition of DMMP (20.2 mM to neat) to this solution; see on the right for the number of molar equivalents of DMMP. (Bottom) Nonlinear least-square analysis of ^{1}H NMR binding data corresponding to the formation of $\mathbf{1}^{6-}\subset$**DMMP** complex. The data, from two measurements (top and bottom), were each fit to 1:1 binding model (SigmaPlot) revealing the formation of a binary complex with stability constants K = 13.9 ± 0.9 M^{-1} / K = 24 ± 1 M^{-1} and random distribution of residuals. The reported value K = 19 ± 7 M^{-1} is an arithmetic mean of two measurements with the standard deviation.

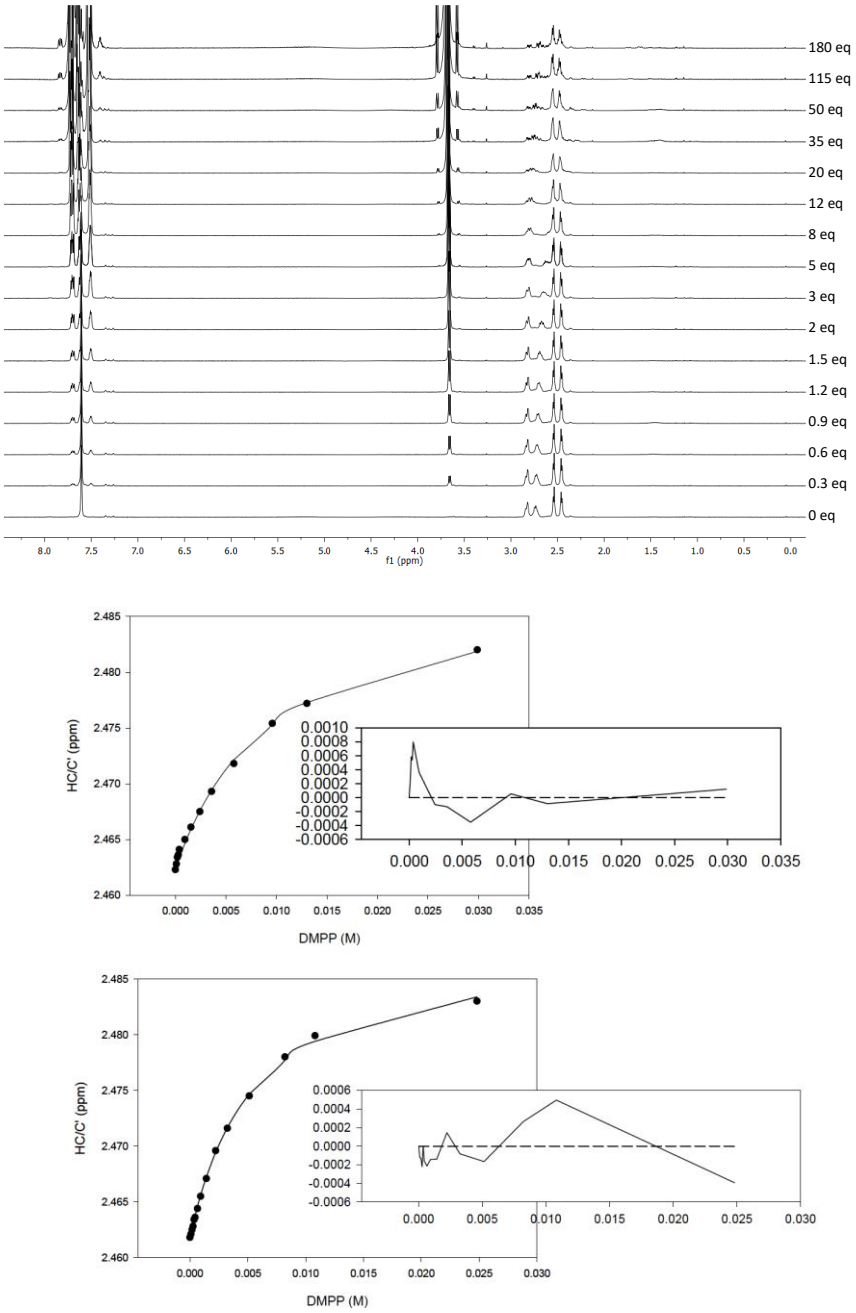

Figure S28. (Top) ^{1}H NMR spectra (700 MHz, 298 K) of 0.3 mM basket $\mathbf{1}^{6-}$ obtained upon incremental addition of DMPP (20.2 mM to neat) to this solution; see on the right for the number of molar equivalents of DMMP. (Bottom) Nonlinear least-square analysis of ^{1}H NMR binding data corresponding to the formation of $\mathbf{1}^{6-}\subset$**DMPP** complex. The data, from two measurements (top and bottom), were each fit to 1:1 binding model (SigmaPlot) revealing the formation of a binary complex with stability constants K = 109 ± 8 M^{-1} / K = 194 ± 7 M^{-1} and random distribution of residuals. The reported value K = 151 ± 60 M^{-1} is an arithmetic mean of two measurements with the standard deviation.

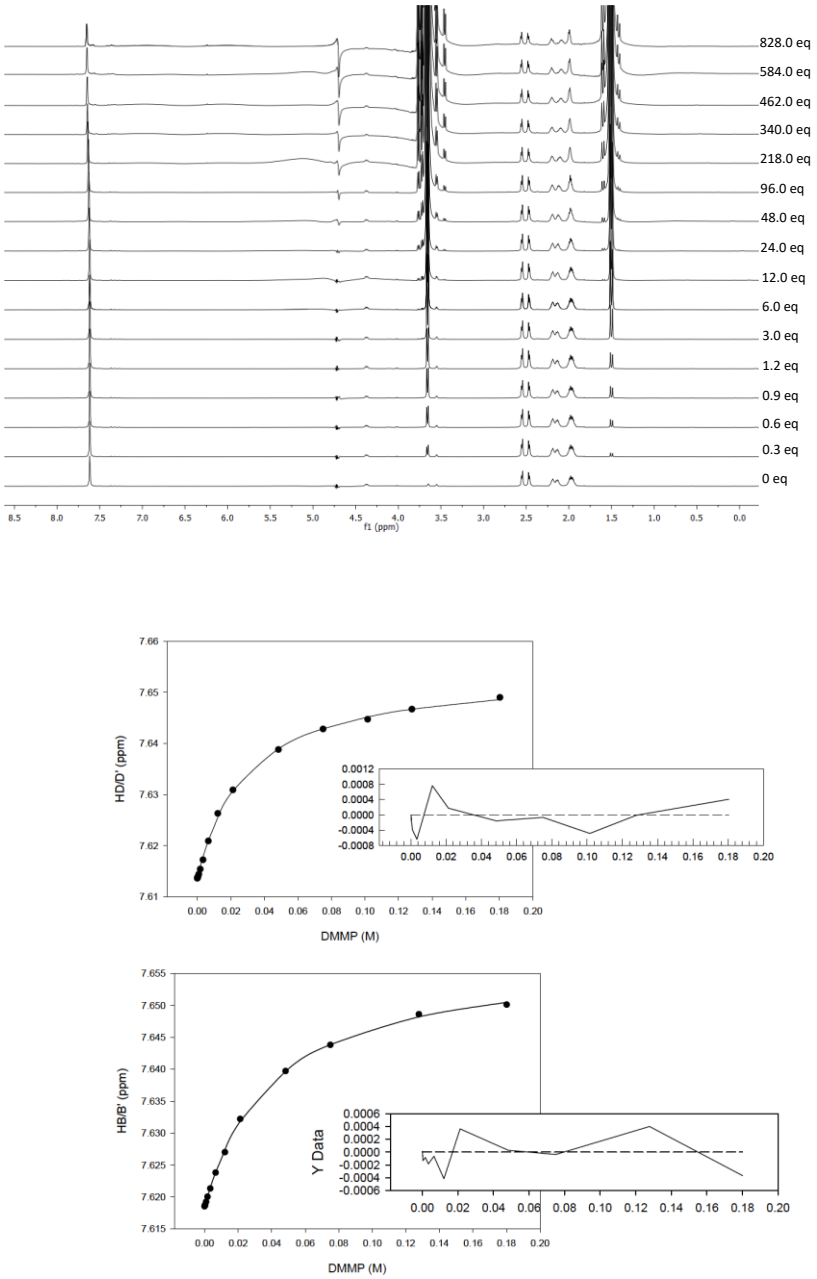

Figure S29. (Top) ^{1}H NMR spectra (700 MHz, 298 K) of 0.3 mM basket $\mathbf{2^{6-}}$ obtained upon incremental addition of DMPP (20.2 mM to neat) to this solution; see on the right for the number of molar equivalents of DMMP. (Bottom) Nonlinear least-square analysis of ^{1}H NMR binding data corresponding to the formation of $\mathbf{2^{6-}}\subset\mathbf{DMMP}$ complex. The data, from two measurements (top and bottom), were each fit to 1:1 binding model (SigmaPlot) revealing the formation of a binary complex with stability constants K = 34 ± 1 M^{-1} / K = 24.3 ± 0.6 M^{-1} and random distribution of residuals. The reported value K = 29 ± 7 M^{-1} is an arithmetic mean of two measurements with the standard deviation.

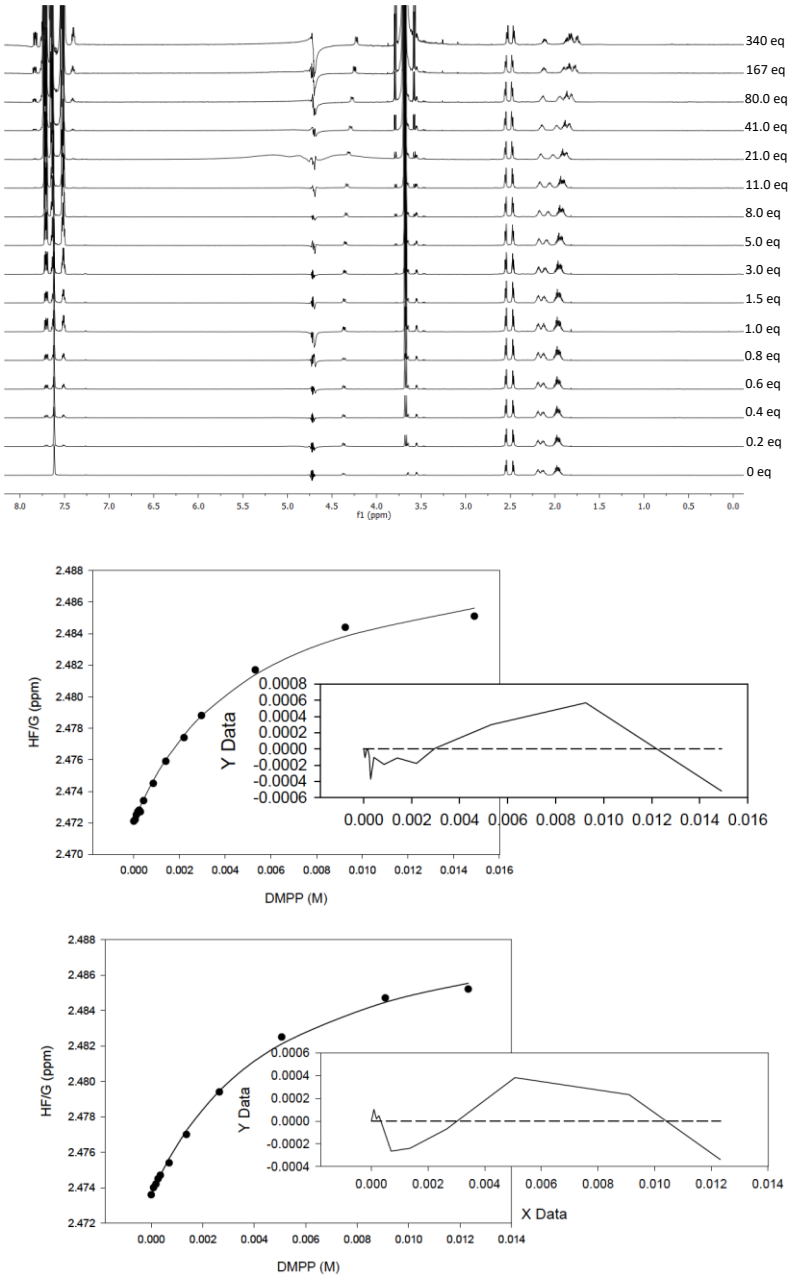

Figure S30. (Top) ^{1}H NMR spectra (600 MHz, 298 K) of 0.3 mM basket $\mathbf{2^{6-}}$ obtained upon incremental addition of DMPP (20.6 mM to neat) to this solution; see on the right for the number of molar equivalents of DMPP. (Bottom) Nonlinear least-square analysis of ^{1}H NMR binding data corresponding to the formation of $\mathbf{2^{6-}}\subset\mathbf{DMPP}$ complex. The data, from two measurements (top and bottom), were each fit to 1:1 binding model (SigmaPlot) revealing the formation of a binary complex with stability constants K = 208 ± 16 M^{-1} / K = 218 ± 17 M^{-1} and random distribution of residuals. The reported value K = 213 ± 7 M^{-1} is an arithmetic mean of two measurements with the standard deviation. Note that one can also fit the data to 1:2 stoichiometric model (basket:DMPP = 1:2) albeit with a similar distribution of residuals to obtain K_1 = 101 M^{-1}/K_2 = 14 M^{-1} and K_1 = 138 M^{-1}/K_2 = 22 M^{-1}.

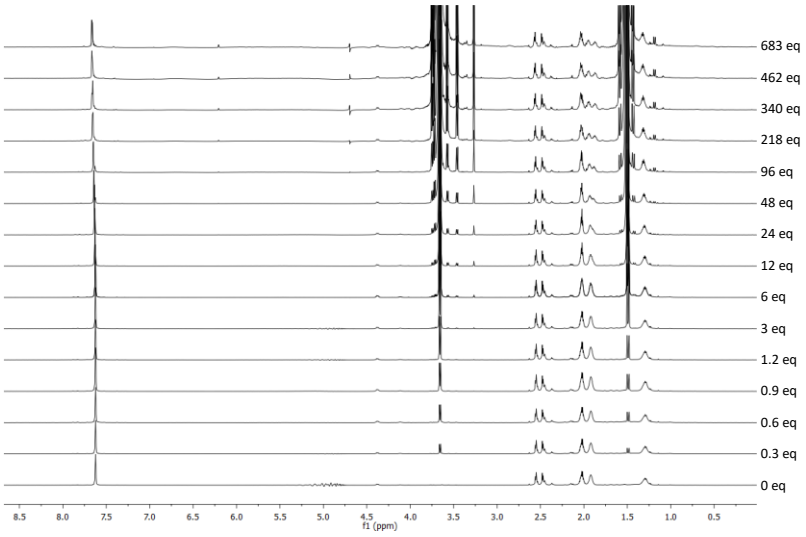

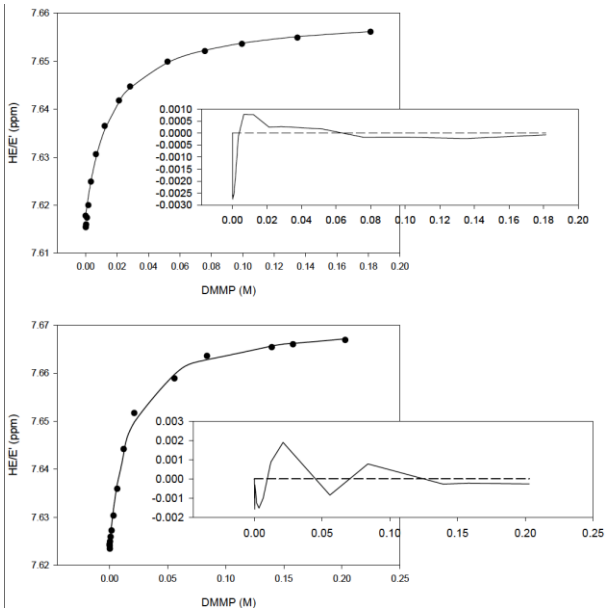

Figure S31. (Top) ^{1}H NMR spectra (700 MHz, 298 K) of 0.3 mM basket $\mathbf{3}^{6-}$ obtained upon incremental addition of DMMP (20.2 mM to neat) to this solution; see on the right for the number of molar equivalents of DMMP. (Bottom) Nonlinear least-square analysis of ^{1}H NMR binding data corresponding to the formation of $\mathbf{3}^{6-}\subset\mathbf{DMMP}$ complex. The data, from two measurements (top and bottom), were each fit to 1:1 binding model (SigmaPlot) revealing the formation of a binary complex with the stability constants $K = 62 \pm 7$ M^{-1} / $K = 57 \pm 4$ M^{-1} and random distribution of residuals. The reported value $K = 59 \pm 4$ M^{-1} is an arithmetic mean of two measurements with the standard deviation.

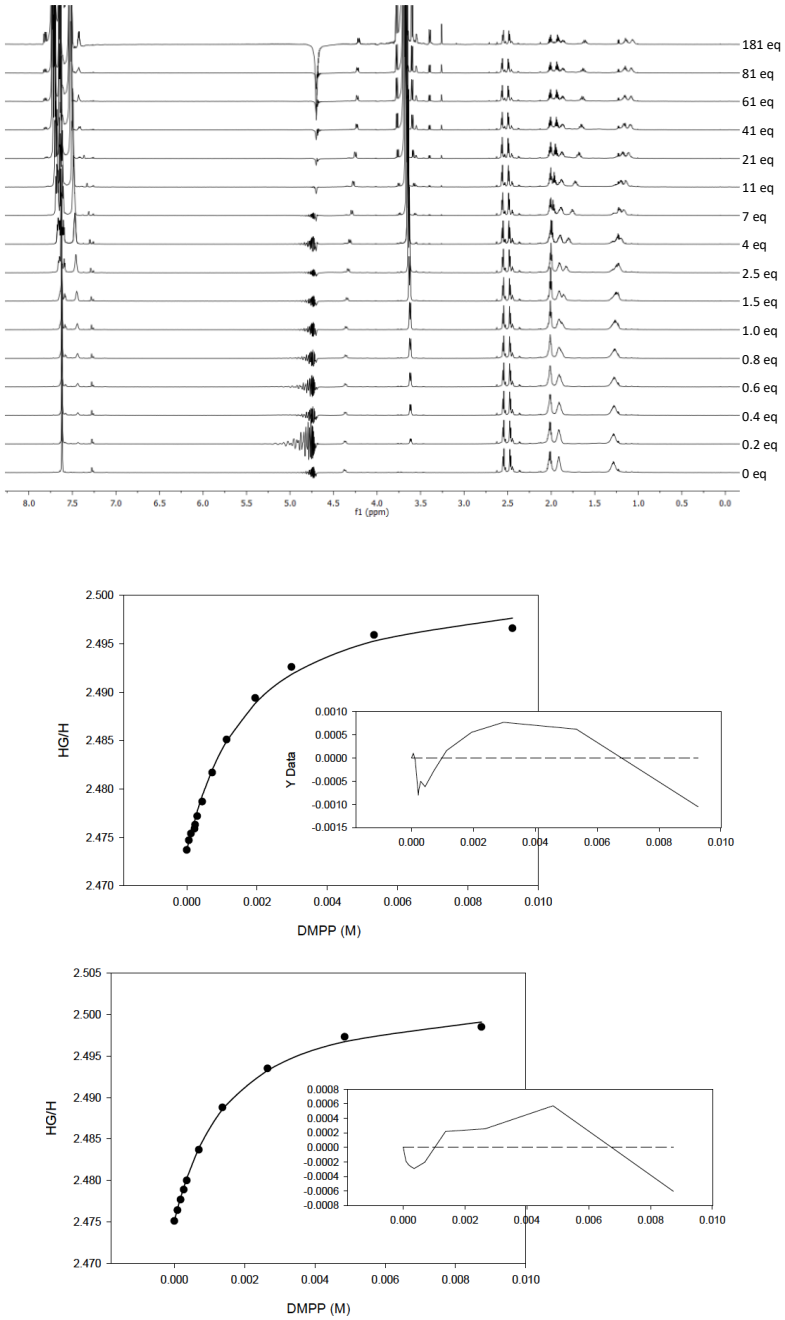

Figure S32. (Top) ^{1}H NMR spectra (600 MHz, 298 K) of 0.3 mM basket $\mathbf{3}^{6-}$ obtained upon incremental addition of DMPP (20.6 mM to neat) to this solution; see on the right for the number of molar equivalents of DMPP. (Bottom) Nonlinear least-square analysis of ^{1}H NMR binding data corresponding to the formation of $\mathbf{3}^{6-}\subset\mathbf{DMPP}$ complex. The data, from two measurements (top and bottom), were each fit to 1:1 binding model (SigmaPlot) revealing the formation of a binary complex with the stability constants K = 659 ± 57 M^{-1} / K = 775 ± 44 M^{-1} and a distribution of residuals that appears not fully randomized. The reported value K = 717 ± 82 M^{-1} is an arithmetic mean of two measurements with the standard deviation. When we fit the data to 1:2 stoichiometric model (basket:DMPP = 1:2), there was a somewhat better distribution of residuals and K_1 = 566 M^{-1}/K_2 = 24 M^{-1} and K_1 = 390 M^{-1}/K_2 = 40 M^{-1}. With $K_1 > K_2$, the first binding event is dominating. If the mean K_1 = 478 M^{-1} value was subsequently incorporated instead of K = 717 ± 7 M^{-1} in Figure 4A, the observed trend would remain the same.

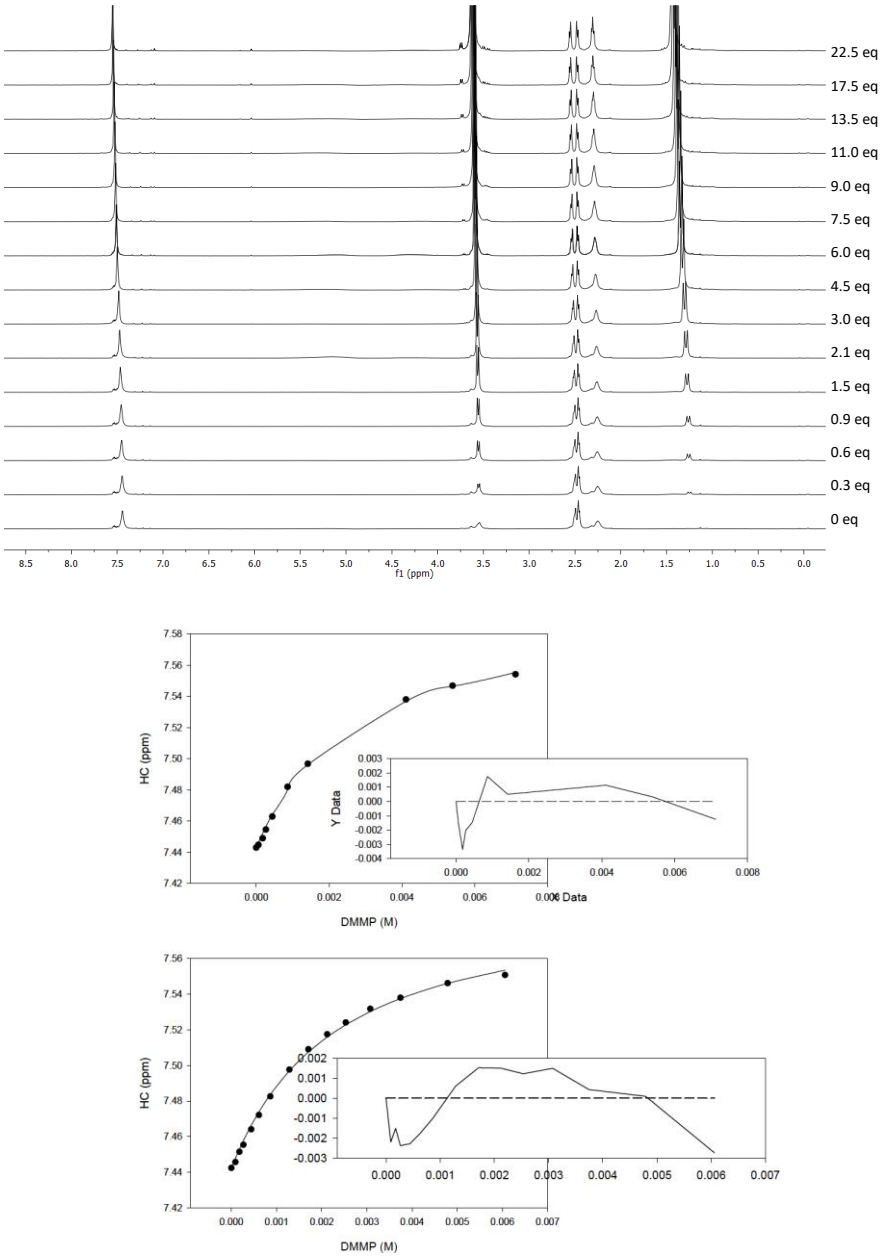

Figure S33. (Top) ^{1}H NMR spectra (600 MHz, 298 K) of 0.3 mM basket $\mathbf{4}^{3-}$ obtained upon incremental addition of DMMP (20.2 mM to neat) to this solution; see on the right for the number of molar equivalents of DMMP. (Bottom) Nonlinear least-square analysis of ^{1}H NMR binding data corresponding to the formation of $\mathbf{4}^{3-}\subset$**DMMP** complex. The data, from two measurements (top and bottom), were each fit to 1:1 binding model (SigmaPlot) revealing the formation of a binary complex with the stability constants K = 411 ± 29 M^{-1} / K = 483 ± 26 M^{-1} and a random distribution of residuals corresponding to the titration isotherm on top. The reported value K = 447 ± 51 M^{-1} is an arithmetic mean of two measurements with the standard deviation. When we fit the data to 1:2 stoichiometric model (basket:DMMP = 1:2), the top isotherm could not be processed due to a poor fitting. For the bottom isotherm, there was a random distribution of residuals and K_1 = 2881 M^{-1}/K_2 = 572 M^{-1}. In this case, the simpler binary model is used to explain the data since it fits reasonably well to the experimental results; even if K_1 = 2881 M^{-1} is used instead of K = 717 ± 82 M^{-1} in Figure 4B, the trend would stay the same.

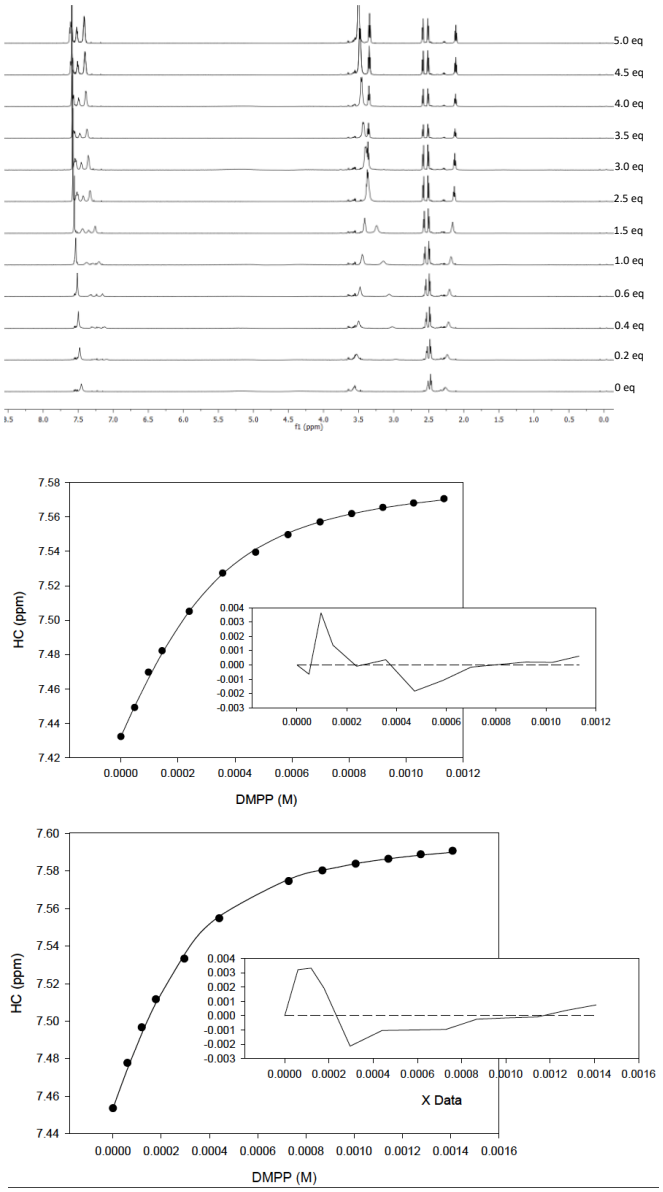

Figure S34. (Top) ^{1}H NMR spectra (700 MHz, 298 K) of 0.3 mM basket $\mathbf{4}^{3-}$ obtained upon incremental addition of DMPP (20.6 mM to neat) to this solution; see on the right for the number of molar equivalents of DMPP. (Bottom) Nonlinear least-square analysis of ^{1}H NMR binding data corresponding to the formation of $\mathbf{4}^{3-}\subset\mathbf{DMPP}$ complex. The data, from two measurements (top and bottom), were each fit to 1:1 binding model (SigmaPlot) revealing the formation of a binary complex with the stability constants K = 8755 ± 544 M^{-1} / K = 9028 ± 78 M^{-1} and a random distribution of residuals. The reported value K = 8891 ± 192 M^{-1} is an arithmetic mean of two measurements with the standard deviation.

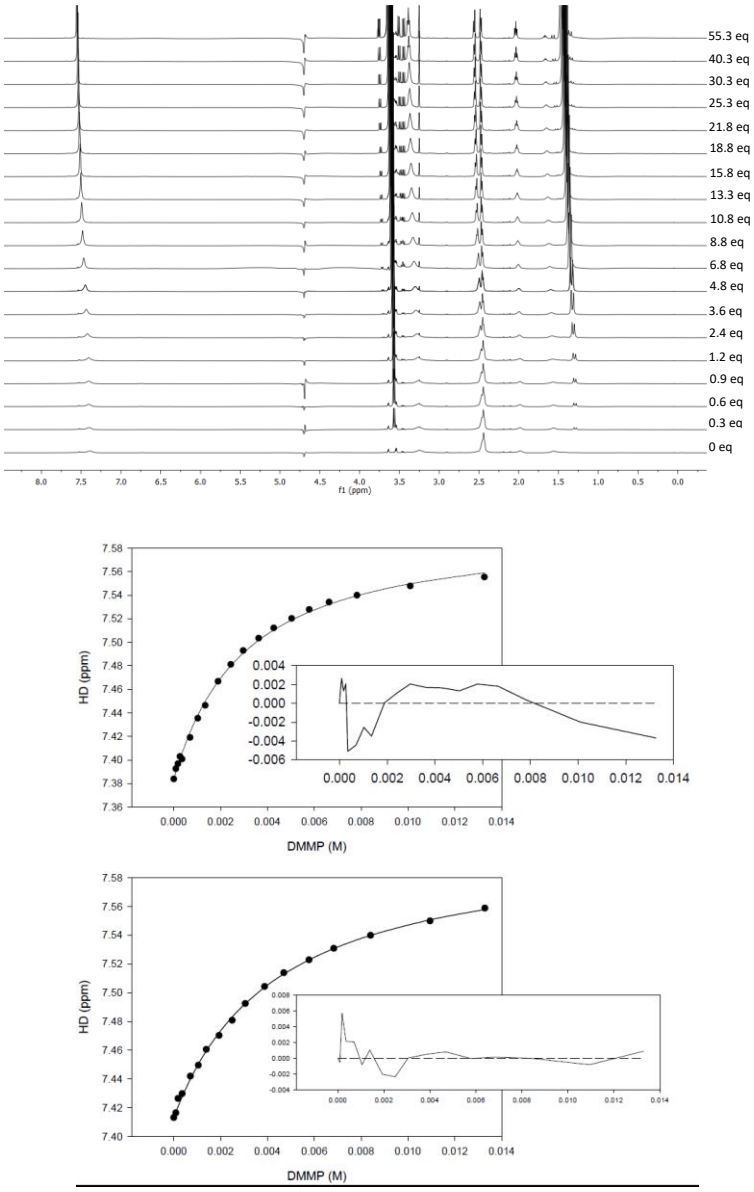

Figure S35. (Top) ^{1}H NMR spectra (600 MHz, 298 K) of 0.3 mM basket $\mathbf{5}^{3-}$ obtained upon incremental addition of DMMP (20.2 mM to neat) to this solution; see on the right for the number of molar equivalents of DMMP. (Bottom) Nonlinear least-square analysis of ^{1}H NMR binding data corresponding to the formation of $\mathbf{5}^{3-}\subset\mathbf{DMMP}$ complex. The data, from two measurements (top and bottom), were each fit to 1:1 binding model (SigmaPlot) revealing the formation of a binary complex with the stability constants K = 385 ± 15 M^{-1} / K = 238 ± 9 M^{-1} and a random distribution of residuals. The reported value K = 311 ± 99 M^{-1} is an arithmetic mean of two measurements with the standard deviation.

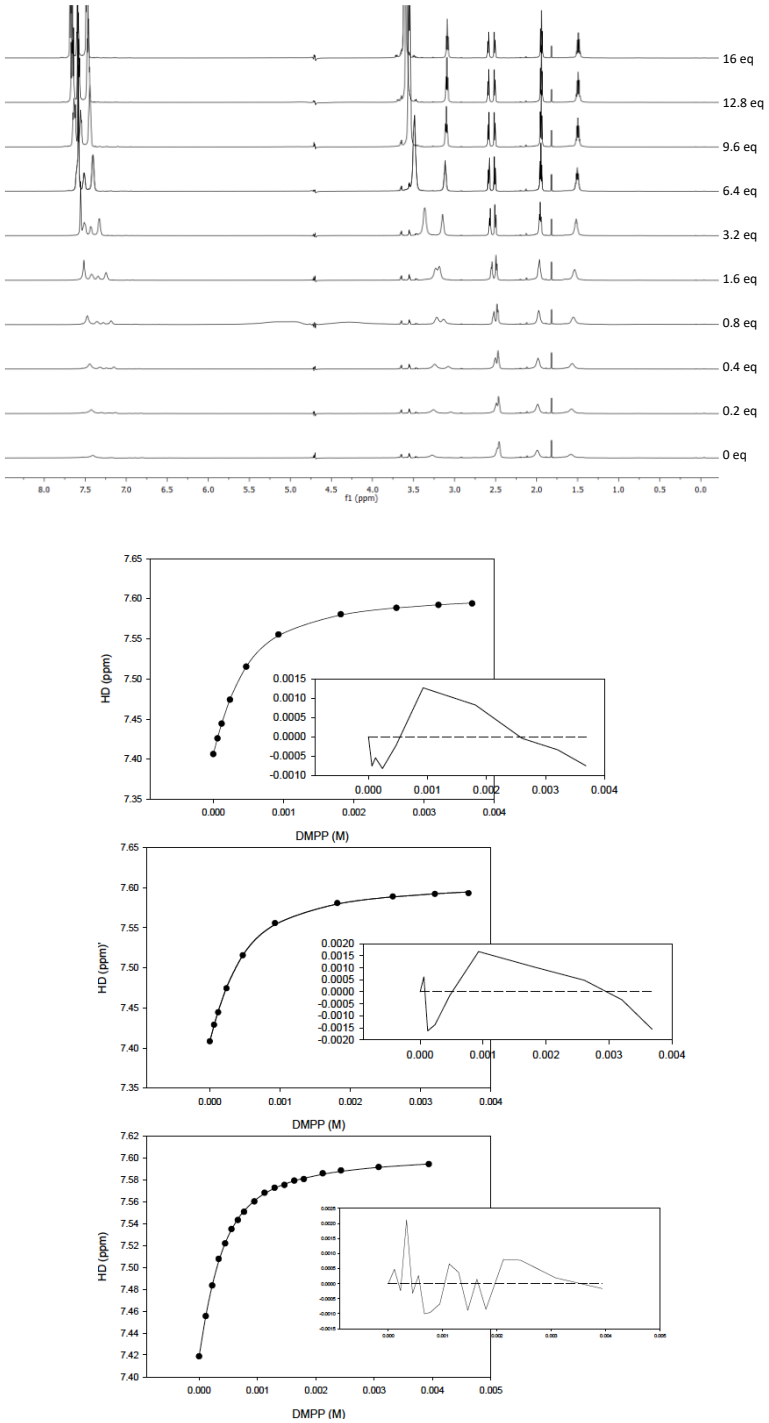

Figure S36. (Top) ^{1}H NMR spectra (600 MHz, 298 K) of 0.3 mM basket $\mathbf{5}^{3-}$ obtained upon incremental addition of DMPP (20.6 mM to neat) to this solution; see on the right for the number of molar equivalents of DMPP. (Bottom) Nonlinear least-square analysis of ^{1}H NMR binding data corresponding to the formation of $\mathbf{5}^{3-}\subset$**DMPP** complex. The data, from three measurements, were each fit to 1:1 binding model (SigmaPlot) revealing the formation of a binary complex with stability constants K = 3742 ± 65 M^{-1} / K = 3675 ± 102 M^{-1}/ K = 4412 ± 68 M^{-1} and a random distribution of residuals corresponding to the last data set. The reported value K = 3943 ± 407 M^{-1} is an arithmetic mean of three measurements with the standard deviation.

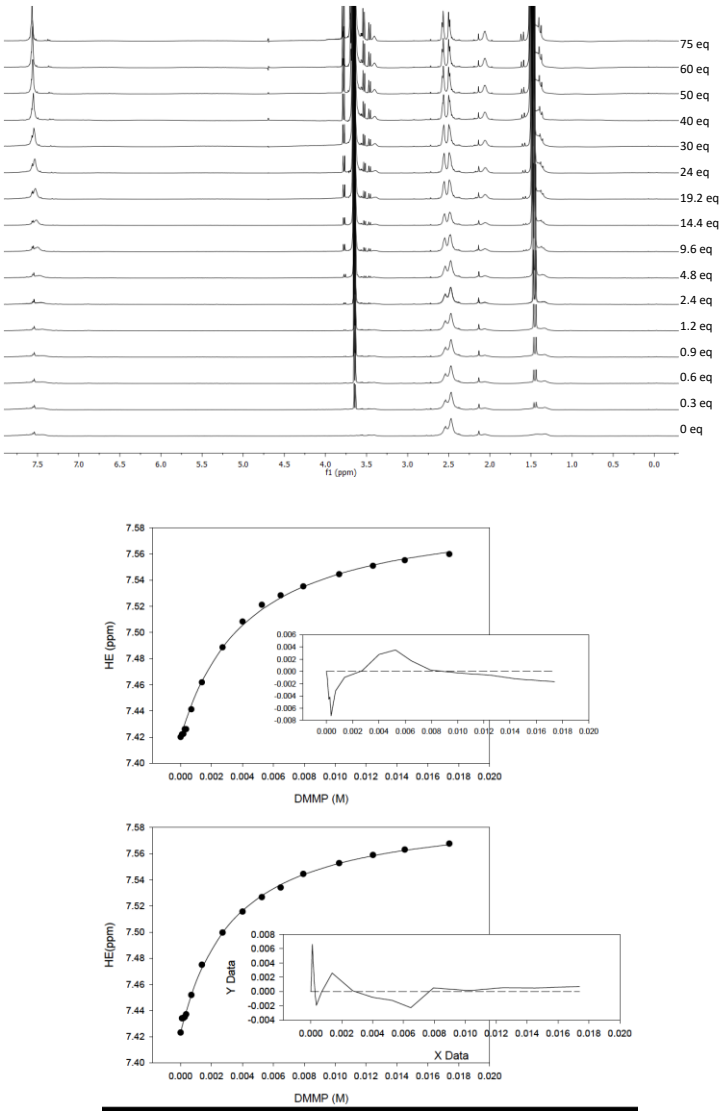

Figure S37. (Top) ^{1}H NMR spectra (700 MHz, 298 K) of 0.3 mM basket $\mathbf{6}^{3-}$ obtained upon incremental addition of DMMP (20.2 mM to neat) to this solution; see on the right for the number of molar equivalents of DMMP. (Bottom) Nonlinear least-square analysis of ^{1}H NMR binding data corresponding to the formation of $\mathbf{6}^{3-}\subset$**DMMP** complex. The data, from two measurements (top and bottom), were each fit to 1:1 binding model (SigmaPlot) revealing the formation of a binary complex with the stability constants K = 247 ± 17 M^{-1} / K = 314 ± 15 M^{-1} and a random distribution of residuals. The reported value K = 280 ± 47 M^{-1} is an arithmetic mean of two measurements with the standard deviation.

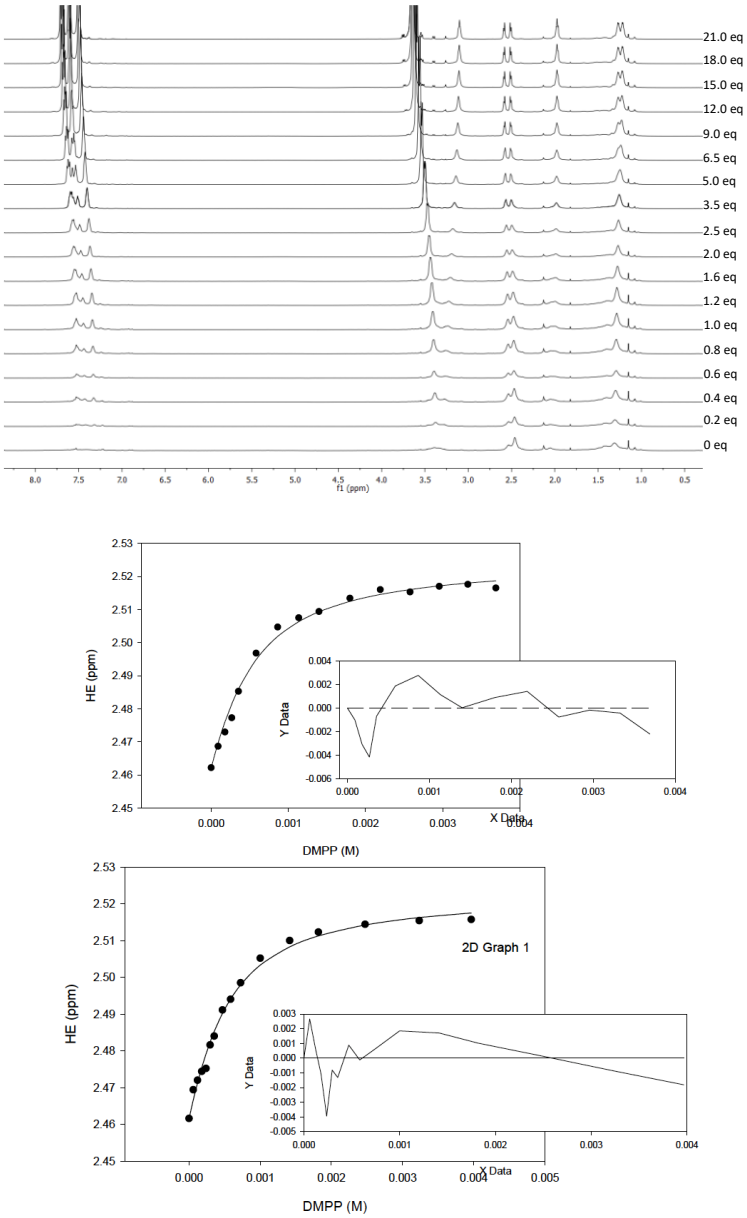

Figure S38. (Top) ^{1}H NMR spectra (700 MHz, 298 K) of 0.3 mM basket $\mathbf{6}^{3-}$ obtained upon incremental addition of DMPP (20.6 mM to neat) to this solution; see on the right for the number of molar equivalents of DMPP. (Bottom) Nonlinear least-square analysis of ^{1}H NMR binding data corresponding to the formation of $\mathbf{6}^{3-}\subset$**DMPP** complex. The data, from two measurements (top and bottom), were each fit to 1:1 binding model (SigmaPlot) revealing the formation of a binary complex with the stability constants K = 2498 ± 287 M^{-1} / K = 2596 ± 234 M^{-1} and a random distribution of residuals. The reported value K = 2547 ± 69 M^{-1} is an arithmetic mean of two measurements with the standard deviation.

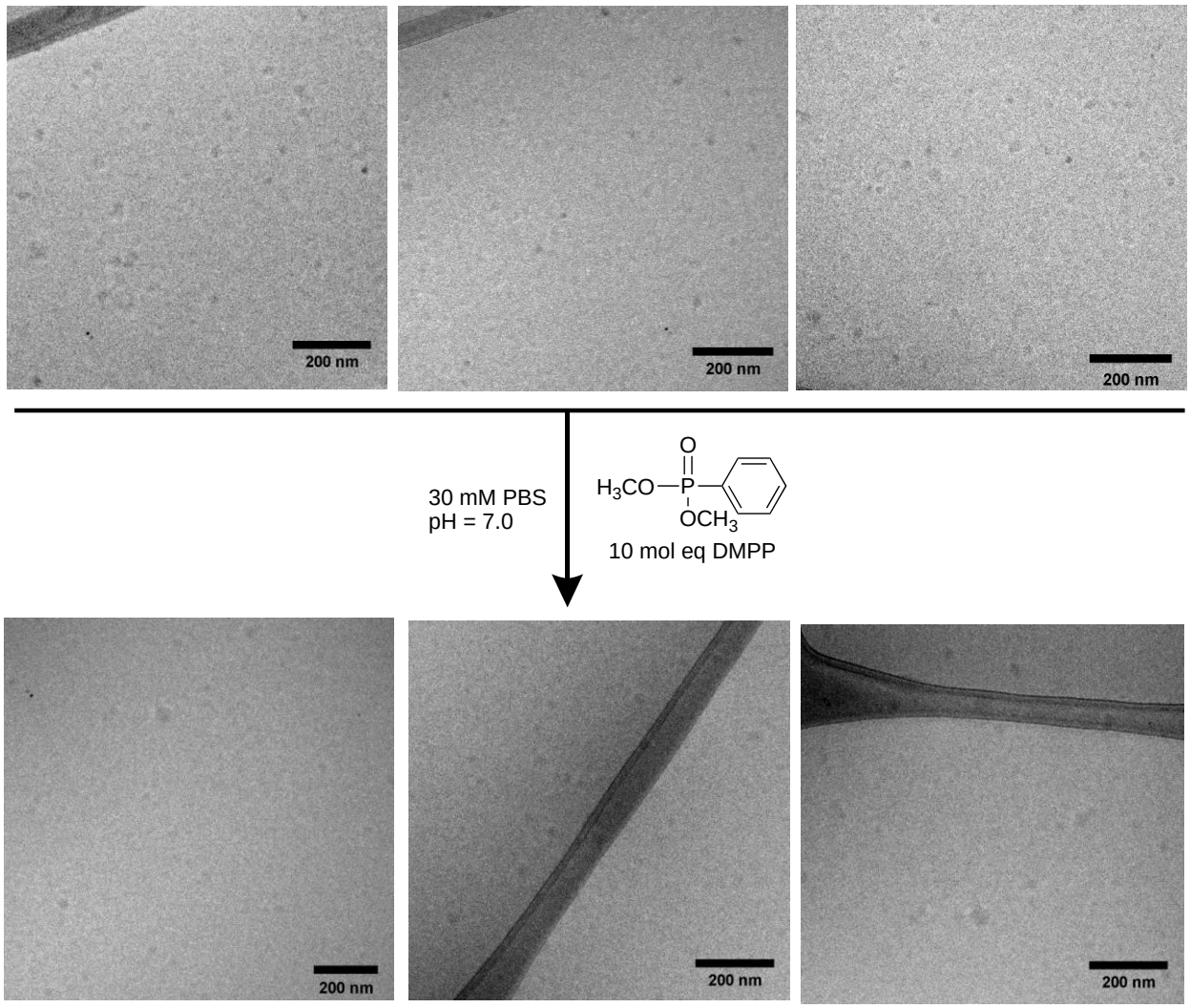

Figure S39. Cryo-TEM images of (top three) 1.0 mM solution of $\mathbf{4}^{3-}$ in 30 mM phosphate buffer at pH = 7.0 and (bottom three) 1.0 mM solution of $\mathbf{4}^{3-}$ in 30 mM phosphate buffer at pH = 7.0 with ten molar equivalents of DMPP. To determine the size of nanoparticles, we randomly chose ten "dots" to obtain their length and height followed by determining the arithmetic mean and standard deviation of such twenty values (see Figure 3B in the main text).

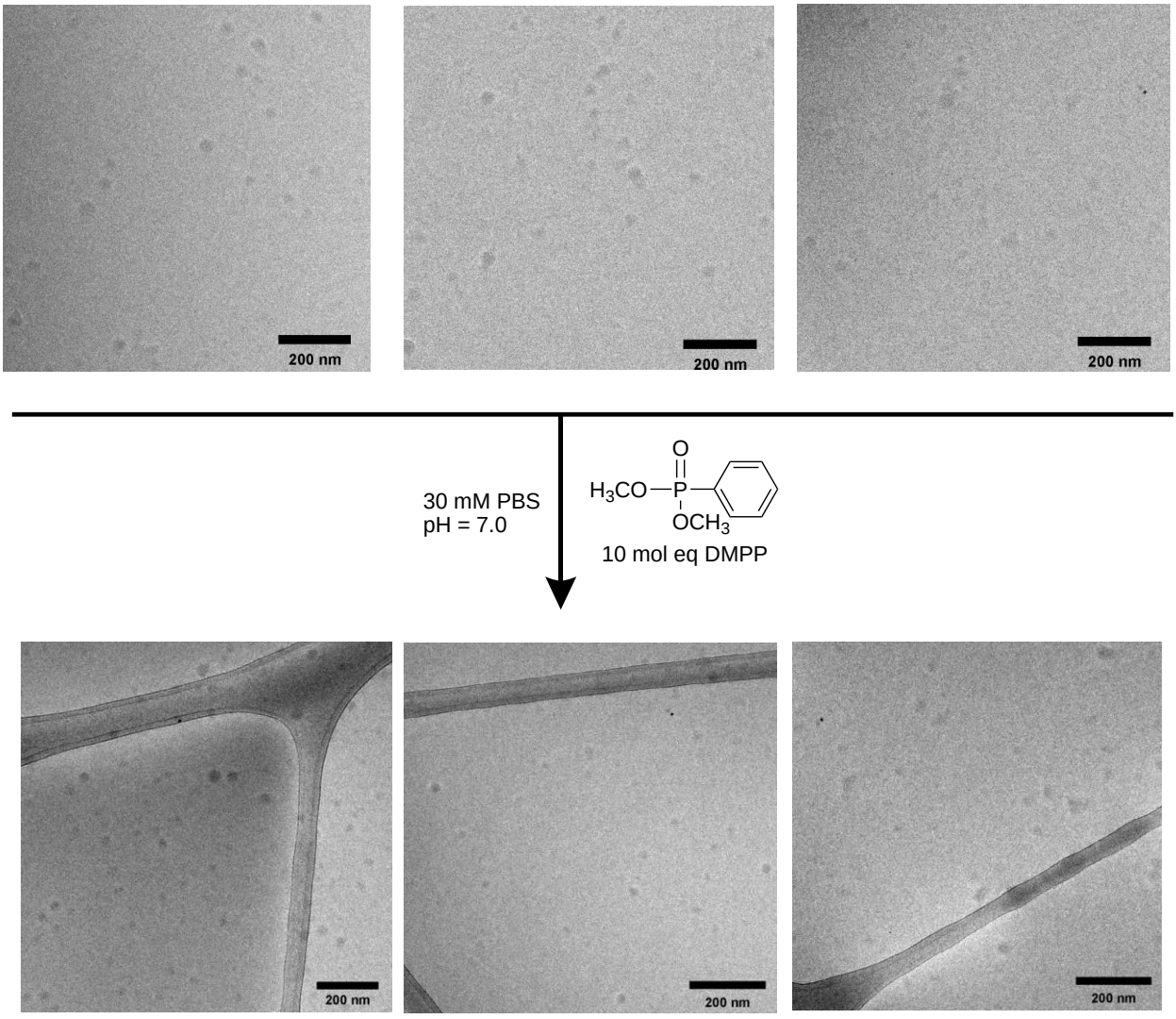

Figure S40. Cryo-TEM images of (top three) 1.0 mM solution of $\mathbf{6}^{3-}$ in 30 mM phosphate buffer at pH = 7.0 and (bottom three) 1.0 mM solution of $\mathbf{6}^{3-}$ in 30 mM phosphate buffer at pH = 7.0 with ten molar equivalents of DMPP. To determine the size of nanoparticles, we randomly chose ten "dots" to obtain their length and height followed by determining the arithmetic mean and standard deviation of such twenty values (see Figure 3B in the main text).

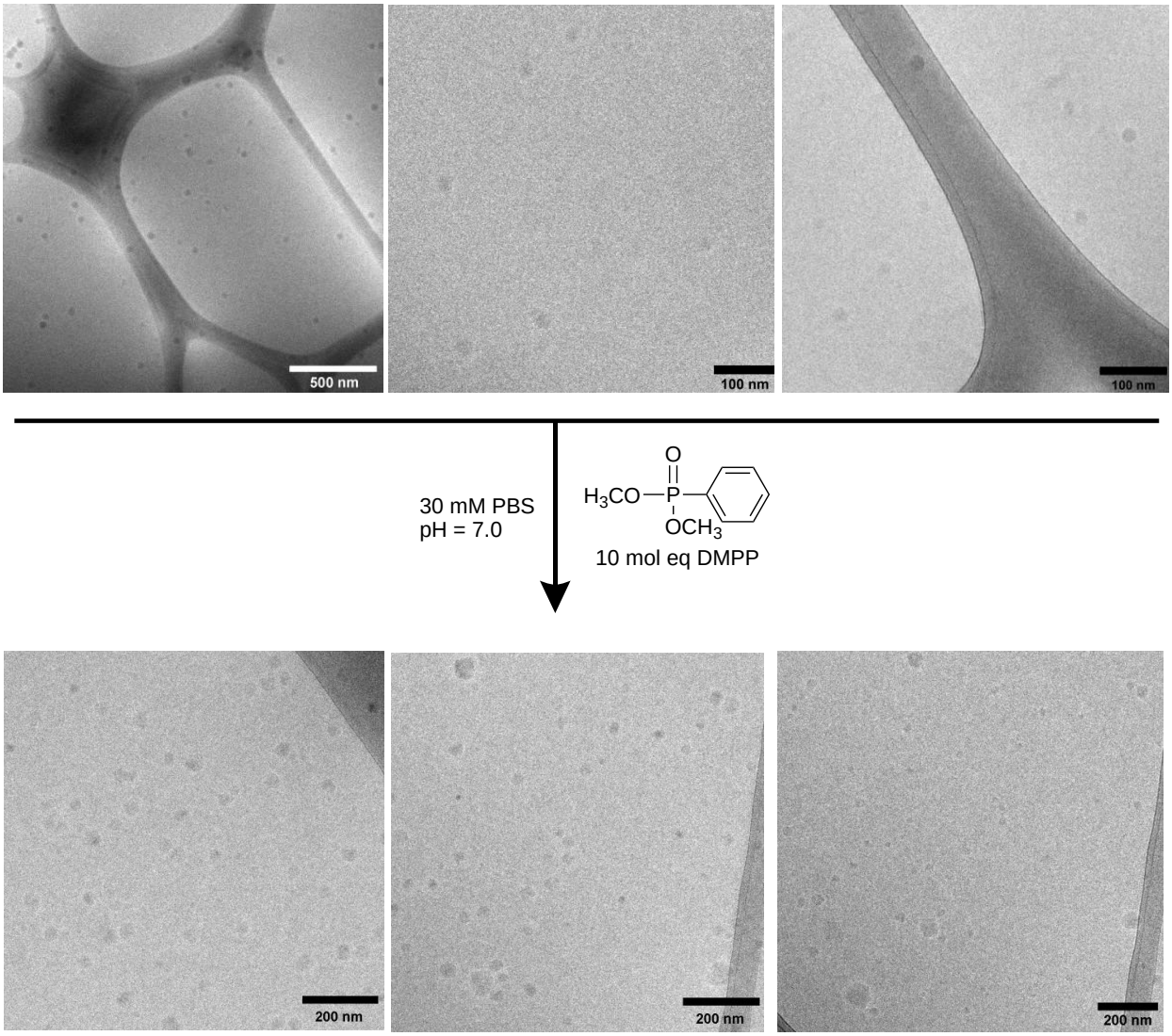

Figure S41. Cryo-TEM images of (top three) 1.0 mM solution of $\mathbf{5}^{3-}$ in 30 mM phosphate buffer at pH = 7.0 and (bottom) 1.0 mM solution of $\mathbf{5}^{3-}$ in 30 mM phosphate buffer at pH = 7.0 with ten molar equivalents of DMPP. To determine the size of nanoparticles, we randomly chose ten "dots" to obtain their length and height followed by determining the arithmetic mean and standard deviation of such twenty values (see Figure 3B in the main text).

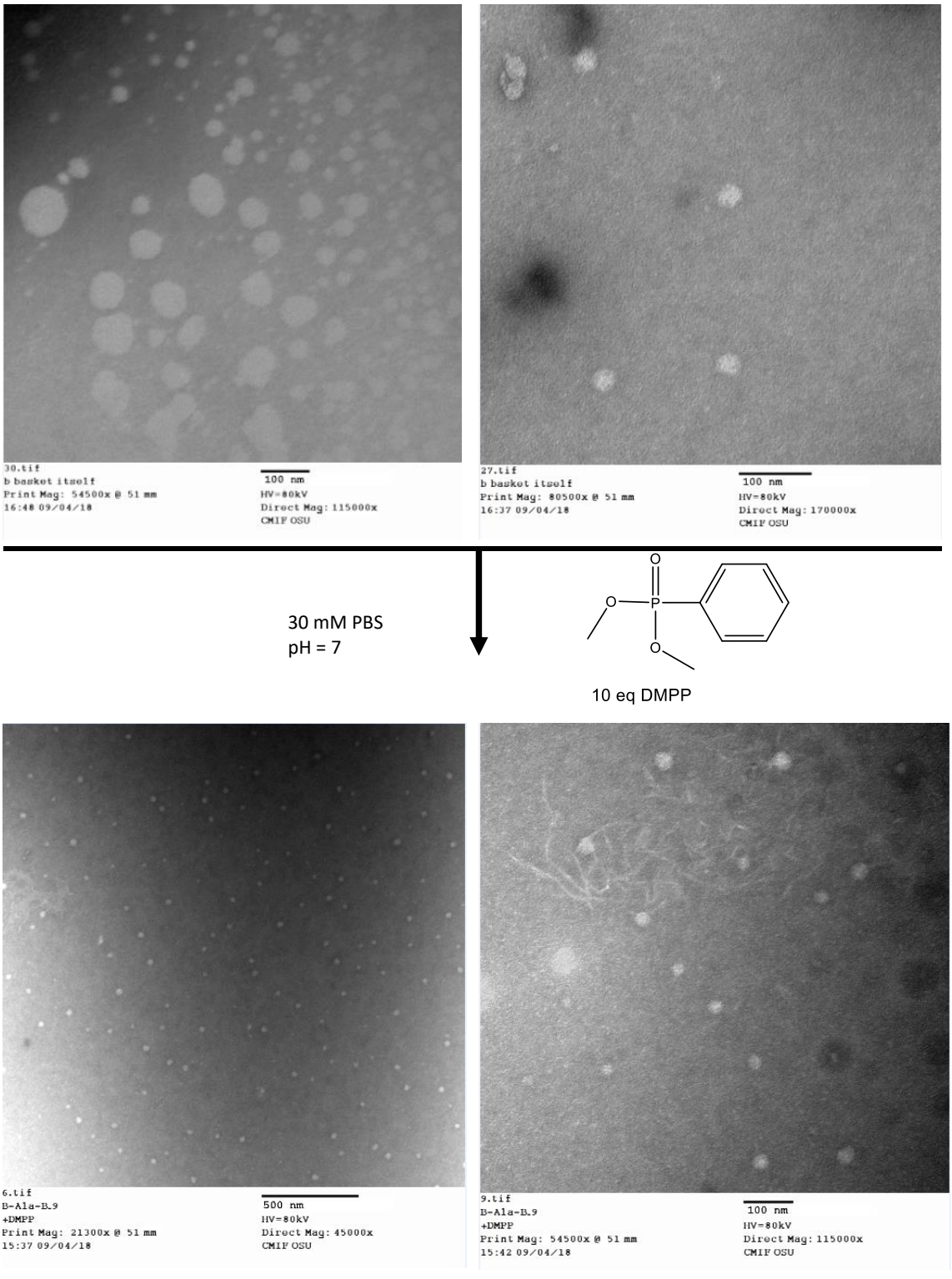

Figure S42. Conventional TEM images of (top two) 1.0 mM solution of $\mathbf{4}^{3-}$ in 30 mM phosphate buffer at pH = 7.0 and (bottom two) 1.0 mM solution of $\mathbf{4}^{3-}$ in 30 mM phosphate buffer at pH = 7.0 with ten molar equivalents of DMPP.

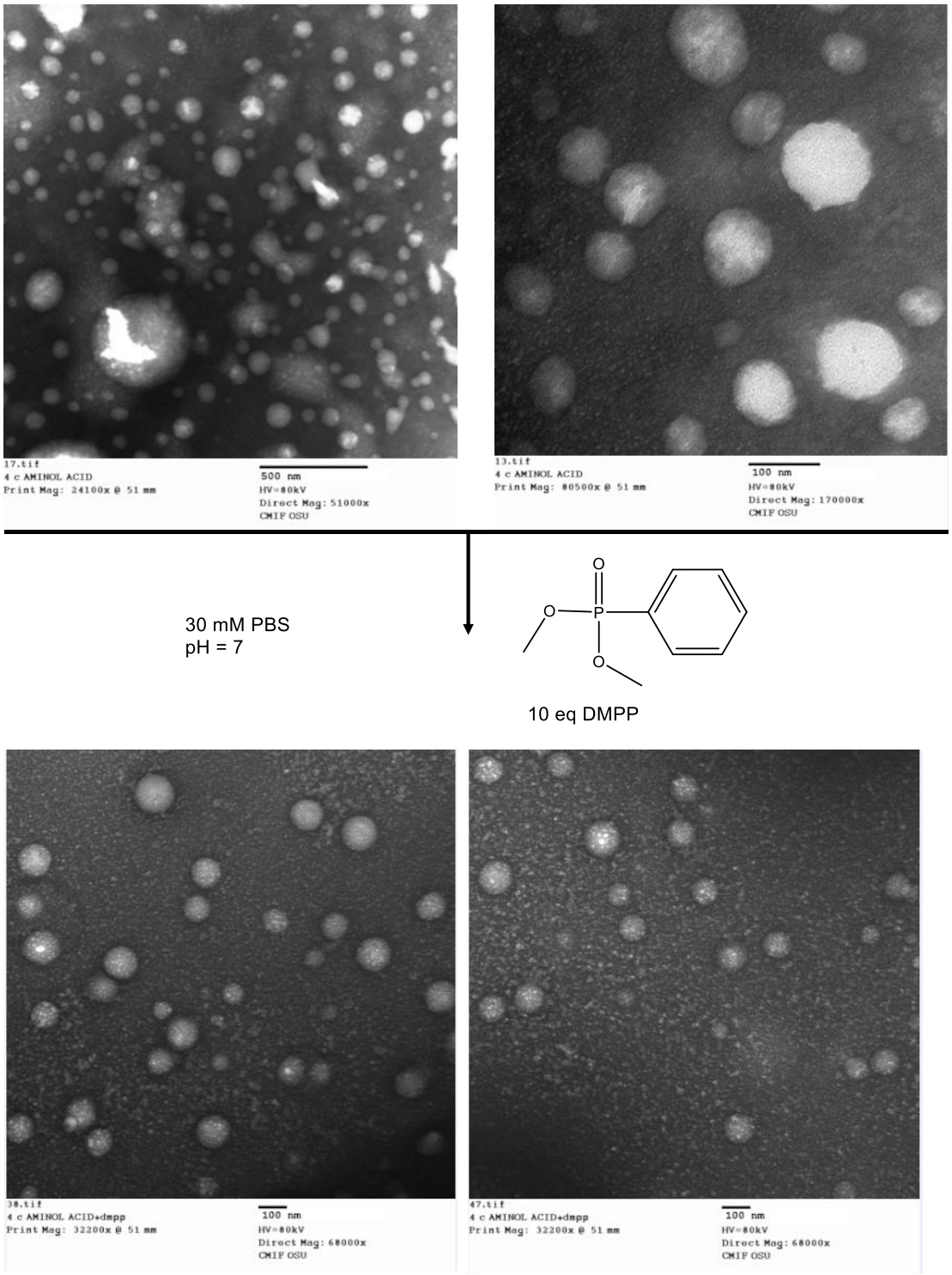

Figure S43. Conventional TEM images of (top two) 1.0 mM solution of $\mathbf{6}^{3-}$ in 30 mM phosphate buffer at pH = 7.0 and (bottom two) 1.0 mM solution of $\mathbf{6}^{3-}$ in 30 mM phosphate buffer at pH = 7.0 with ten molar equivalents of DMPP.

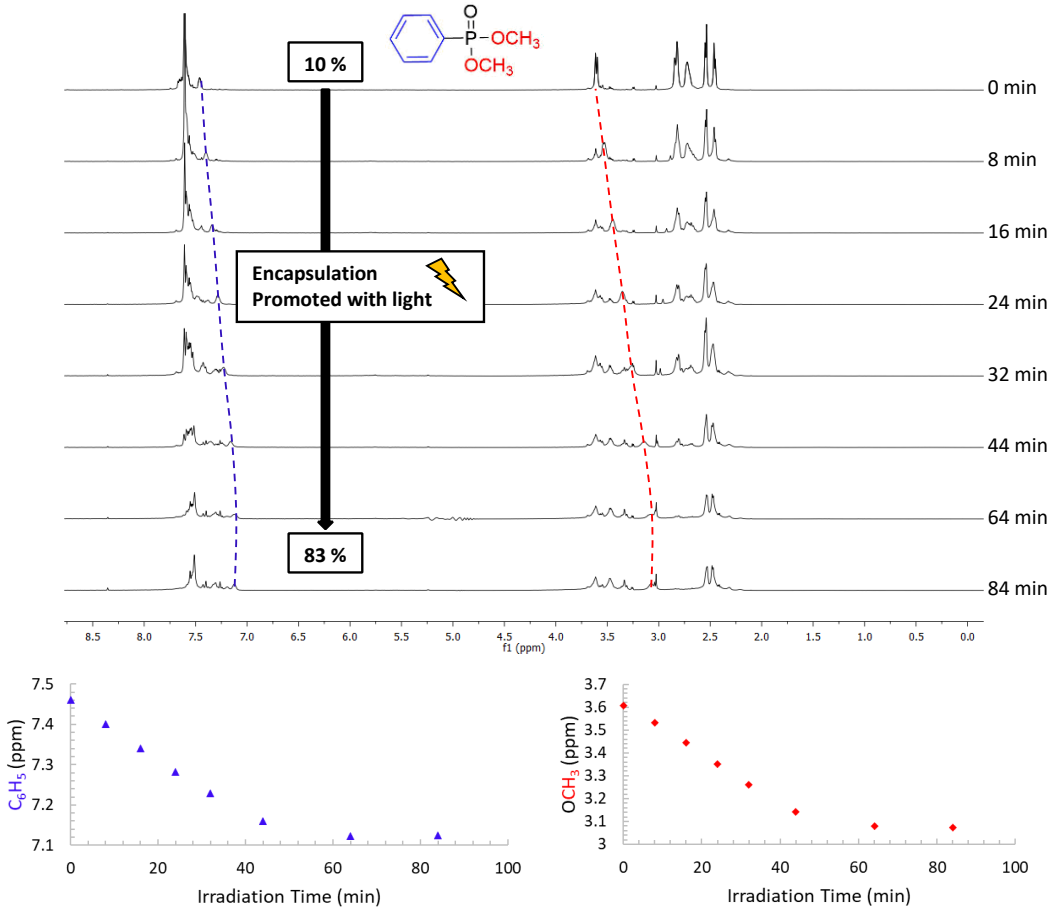

Figure S44. ^{1}H NMR spectra (700 MHz, 298.0 K) of 0.8 mM solution of $\mathbf{1}^{6-}$ with 0.4 molar equivalents of DMPP (30.0 mM phosphate buffer at pH = 7.0 ± 0.1) obtained upon irradiation at 300 nm; note that times at which the spectra were taken are shown on the right. A standard solution of $\mathbf{1}^{6-}$ was prepared in 30.0 mM phosphate buffer (containing 20% of D_2O) at pH 7.0 ± 0.1; the pH of the solution was adjusted to 7.0 using 0.3 M NaOH. 500 µL of this solution, contained in an NMR tube, was placed inside a Rayonet reactor to maintain a constant temperature of 35˚C (fan). The samples were irradiated at 300 nm (sixteen 3000Å bulbs distributed symmetrically around the chamber). At certain time intervals, we would remove the NMR tube from the reactor to record ^{1}H NMR spectrum (water suppression NMR pulse sequence for saturating the signal of the solvent). Note: the methoxy and an aromatic resonance of DMPP are highlighted with a red asterisk at each time point.

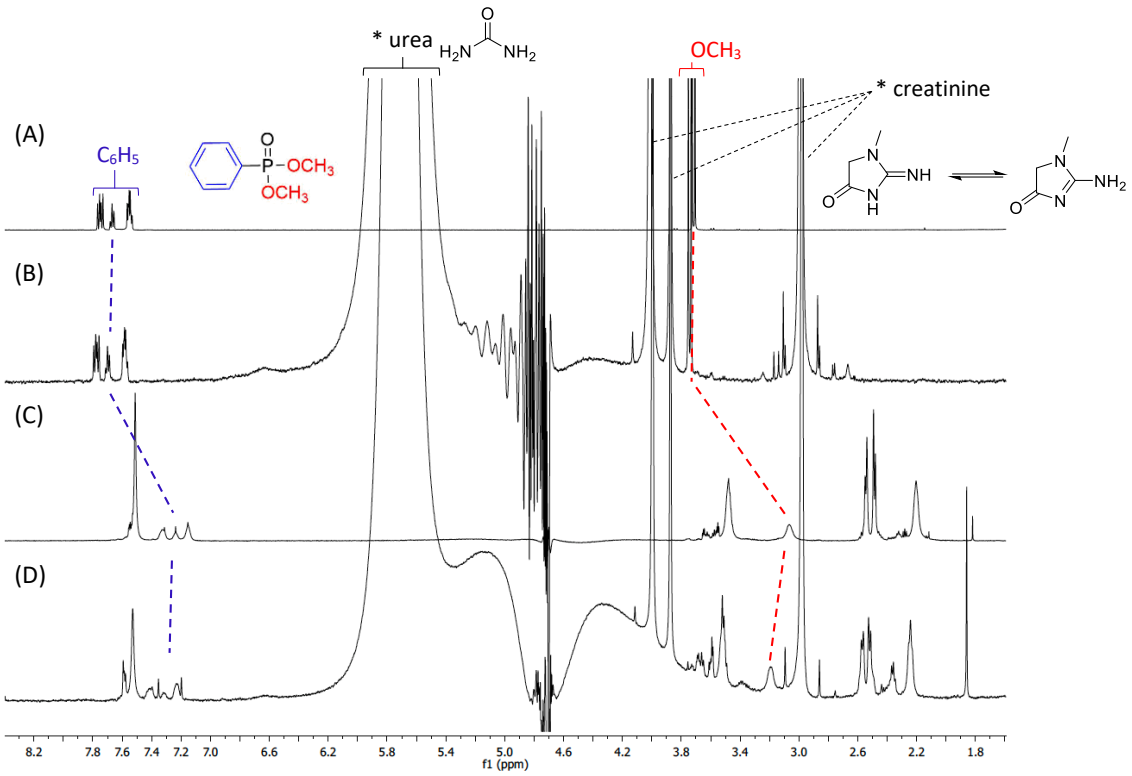

Figure S45. ^{1}H NMR spectra (600 MHz, 298 K) of, from top to bottom: (a) 0.2 mM DMPP in PBS buffer at pH = 7.0, (b) 0.2 mM DMPP in Surine, (c) 0.3 mM $\mathbf{4}^{3-}$ in 30 mM PBS buffer at pH = 7.0 containing 0.2 mM DMPP and (d) 0.3 mM $\mathbf{4}^{3-}$ in Surine containing 0.2 mM DMPP.

Computational Studies

The Monte-Carlo (MC) conformational sampling of $\mathbf{1}^{6-}$ and $\mathbf{3}^{6-}$ was completed with the Maestro suite (Schrodinger) using OPLS3 molecular mechanics (MM) force field in implicit H_2O solvent. For each search, we used systematic torsional sampling method with 200 steps per rotatable bond and 50,000 steps overall. The energy window for saving structures was set to 50 kJ/mol.

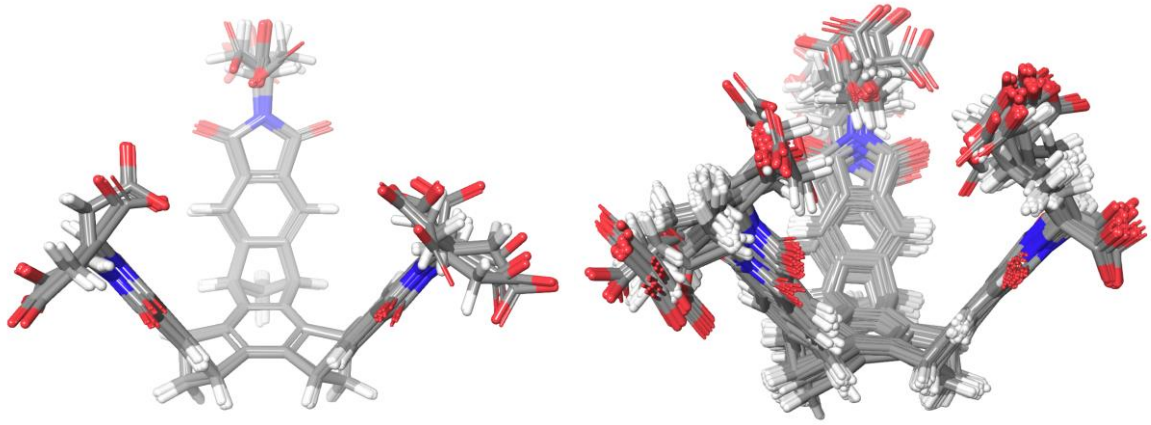

Figure S46. For capsule $\mathbf{1}^{6-}$, the MCMM search gave 100 unique conformers of which 10 within 5 kcal/mol are shown on the left. For capsule $\mathbf{3}^{6-}$, the MCMM search gave 5019 unique conformers of which 33 within 2 kcal/mol are shown on the right.

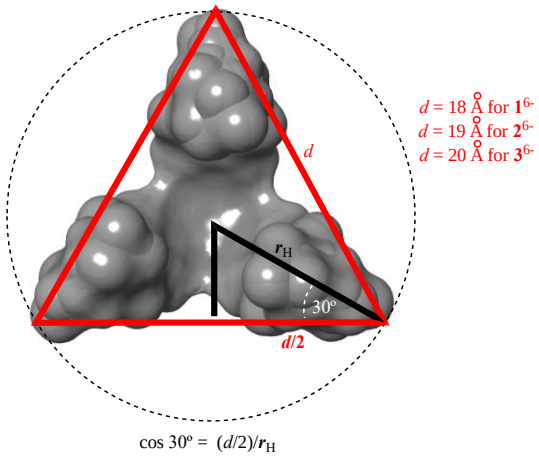

Figure S47. To estimate hydrodynamic radii $\boldsymbol{r}_H$ of $\mathbf{1}^{6-}$, $\mathbf{2}^{6-}$ and $\mathbf{3}^{6-}$ (Figure 3B) we used distance d between terminal carboxylates of fully extended baskets (MCMM calculation results, Figure S42). Following, we used the following equation $cos\ 30^o = (d/2)/\boldsymbol{r}_H$ to calculate $\boldsymbol{r}_H$, as shown in Figure 3B.

Reference

(1) Border, S. E.; Pavlović, R. Z.; Zhiquan, L.; Badjić, J. D. Removal of Nerve Agent Simulants from Water Using Light-Responsive Molecular Baskets. *J. Am. Chem. Soc.* **2017**, *139* (51).